Exhibiting Singularity-Free Ultra-Compact Stellar Models in Teleparallel $f(\mathfrak{T})$ Gravity Under the MIT Bag EoS *

H. Nazar[1†] G. Abbas[2,3‡] M. R. Shahzad[4,5§] Tayyab Naseer[6♮] Jawaher Saud Alrashood[7♯] Walid Abdelfattah[8¶]

[1]Research Center of Astrophysics and Cosmology, Khazar University, Baku, AZ1096, 41 Mehseti Street, Azerbaijan
[2]Department of Mathematics, The Islamia University of Bahawalpur, Bahawalpur, Pakistan
[3]Jadara University Research Center, Jadara University, P.O. Box 733, Irbid 21110, Jordan
[4]Institute for Theoretical Physics and Cosmology, Zhejiang University of Technology, Hangzhou 310023, China
[5]Department of Mathematics, Bahauddin Zakariya University, Vehari Campus, Vehari 61100, Pakistan
[6]Department of Mathematics, University of Okara, Okara 56300, Pakistan
[7]Department of Teaching and Learning, College of Education and Human Development, Princess Nourah bint Abdulrahman University, P. O. Box 84428, Riyadh 11671, Saudi Arabia
[8]Humanities and Social Research Center, Northern Border University, Arar, Saudi Arabia

Abstract: This paper presents a relativistic model of anisotropic strange quark stars in teleparallel $f(\mathfrak{T})$ gravity, in which the stellar interior contains an anisotropic fluid distribution. The analysis begins with the modified gravitational field equations for a linear $f(\mathfrak{T})$ model in a static spherically symmetric spacetime geometry. Physically viable solutions are obtained using an interior configuration modeled with the MIT Bag model equation of state (EoS) and the Finch--Skea spacetime ansatz, yielding a self-consistent stellar solution. The exterior Schwarzschild spacetime is smoothly matched to the interior geometry at the stellar boundary, and the model parameters are determined from the continuity conditions. The resulting solution is further examined using thermodynamic, energy, and stability criteria for physical viability. Its observational relevance is evaluated for the compact stars $SAX\,J1808.4-3658$ and $4U\ 1608-52$. The derived solutions show that, under appropriate parameter choices for the $f(\mathfrak{T})$ model, the proposed strange quark star configuration may be realized with higher values of mass and compactness, which may have implications for astrophysics in the context of modified teleparallel gravity. The results indicate that $f(\mathfrak{T})$ gravity can provide an effective description equivalent to General Relativity, accompanied by a modified coupling and a constant geometric contribution, thereby offering a possible framework for exploring the behavior of highly compact strange quark stars.

Keywords: Exact solutions, anisotropic quark matter, structural stability, compact objects, teleparallel gravity

DOI: 10.1088/1674-1137/aebb0e **CSTR:**

CPC Accepted

I. INTRODUCTION

It is widely acknowledged that Einstein's theory of general relativity (GR), which describes gravity in terms of spacetime curvature, has consistently proven to be an extraordinarily successful and reliable model across a wide range of energy scales. To date, none of its predictions has failed experimental testing. However, several open theoretical questions persist, including the cosmological constant problem [1] and the inability to account for the universe's accelerating expansion [2]. These difficulties have motivated the development of alternative frameworks that aim to resolve such issues, describe gravitational behavior on cosmological and astrophysical scales, and recover the predictions of GR in appropriate limits [3−8]. Among the simplest alternatives to GR is the widely studied $f(R)$ theory [7], in which the gravitational Lagrangian is a general function of the Ricci scalar R. Re-

Received 27 August 2026; Accepted 26 October 2026

* The authors also extend their appreciation to the Deanship of the Scientific Research at Northern Border University, Arar, KSA Saudi Arabia, for supporting this work through the project number (NBU-FFR-2026-2230-20). The authors also express their gratitude to Princess Nourah bint Abdulrahman University Researchers Supporting Project number (PNURSP2026R581), Princess Nourah bint Abdulrahman University, Riyadh, Saudi Arabia

† E-mail: hammadnazar350@gmail.com, hamad.nazar@khazar.org (Corresponding author)
‡ E-mail: ghulamabbas@iub.edu.pk
§ E-mail: dr.rizwanshahzad@bzu.edu.pk
♮ E-mail: tayyabnaseer48@yahoo.com (Corresponding author)
♯ E-mail: gsalrshod@pnu.edu.sa
¶ E-mail: walid.abdelfattah@nbu.edu.sa

©2027 Chinese Physical Society and the Institute of High Energy Physics of the Chinese Academy of Sciences and the Institute of Modern Physics of the Chinese Academy of Sciences and IOP Publishing Ltd. All rights, including for text and data mining, AI training, and similar technologies, are reserved.

cently, a range of problems within this gravitational framework has been explored in different settings, from simulations of cosmic phenomena to models of dense astrophysical objects [9−21]. Another alternative to standard gravity that has recently attracted considerable interest is $f(T)$ gravity. The development of this theory was motivated by the formulation of $f(R)$ gravity, in which the gravitational description typically depends on the scalar curvature R of the underlying geometry [22−27]. Like its $f(R)$ counterpart, $f(T)$ gravity represents an extended or generalized formulation. $f(T)$ gravity is based on the teleparallel equivalent of GR ($TEGR$) [28−30], in which the Lagrangian depends on the torsion scalar T [31,32]. In both GR and its teleparallel equivalent, the basic field equations satisfy the relation $R=-T+B$, where $B=\frac{2}{e}\partial_\mu(eT^\mu)$ represents a term that is a total derivative and a function only of T. Consequently, the action may be expressed in terms of either R or T, and both choices yield identical field equations for GR and its teleparallel counterpart [33,34]. Thus, the formal framework of $f(T)$ gravity requires a definite choice of the tetrad-field configuration. The choice of tetrad is important in investigating the model because $f(T)$ gravity is not invariant under local Lorentz transformations. As a torsion theory, $TEGR$ is comparable to GR, but $f(T)$ is not.

During the evolutionary stages of a typical star, ultracompact objects can form. This stage marks the onset of gravitational collapse: the outward pressure from ongoing thermonuclear fusion reactions inside the star is no longer sufficient to counterbalance the inward pull of gravity. As a result of this collapse, also referred to as stellar death, a new entity known as a compact object is formed. Thermonuclear fusion ceases during this phase when all helium sources are exhausted. Consequently, the star's internal pressure rises and its thermal conductivity decreases. The object's entire mass is compressed to an extremely high density as a result of this increase in internal pressure. Compared with ordinary stars, compact objects have significantly smaller radii and extremely high densities. Some of the most remarkable achievements in astrophysics involve extremely dense compact objects, including quark stars, neutron stars, pulsars, and several other rapidly rotating celestial bodies characterized by strong magnetic interactions. Compact objects are believed to be composed of small subatomic particles, including mesons, baryons, exotic quarks, and leptons. Nevertheless, precise experimental information regarding the formation of these ultra-dense objects is currently lacking. Therefore, one of the main challenges in modeling the structure of these objects lies in identifying an appropriate geometry and accurately describing the matter distribution within their interiors. Within the framework of $f(T)$ gravity theories, which can accommodate a range of physical constraints, several significant results concerning the description of compact stellar objects have recently been reported [35−43]. The literature [44−57] also contains many well-established findings regarding the formation of astrophysical compact objects within other modified gravity theories.

Given these distinctive implications, teleparallel gravity theories have been employed to study certain properties of stellar compact objects, including strange stars, black holes, and neutron stars [58−67]. Physicists typically focus on pressure isotropy when modeling compact objects. However, recent investigations of specific stellar compact objects, including $4U1538-52$, $4U1820-30$, and $PSRJ1614-2230$, indicate that their internal structures are composed of anisotropic fluids. The presence of anisotropic fluid configurations in these stars can be attributed to various mechanisms, such as superfluid components, rotation, stellar evolution, viscous effects, magnetic fields, and dense cores spanning a wide range of masses. Bahamonde and collaborators [68] studied the possible properties of anisotropic stars under diverse physical conditions within symmetric teleparallel gravity theories. Said and Solanki [69] investigated a novel set of exact solutions to the spherically symmetric field equations in $f(T)$ gravity, aimed specifically at describing anisotropic neutron stars. To derive analytical solutions under the quadratic $f(T)$ formulation, the investigators used an off-diagonal tetrad and adopted geometrically plausible variables. The resulting solutions can faithfully represent a broad spectrum of compact stellar configurations. Within the framework of symmetric teleparallel gravity, Ditta and his collaborators [70] analyzed the influence of the quintessence field on anisotropic compact objects by means of an embedding class-one approach. Daouda and collaborators [71] presented a procedure for identifying anisotropic features in spherically symmetric geometries through the use of off-diagonal tetrads within the teleparallel framework. Using a non-diagonal tetrad, Abbas and Zubair [72] obtained analytical solutions to the $f(T)$ field equations for anisotropic strange-star models. Saridakis and Nashed [73] applied a perturbative method within the $f(T)$ framework to investigate various physical aspects related to the stability and thermodynamic behavior of spherically symmetric charged black holes. Deb and collaborators [74] explored exact solutions to the generalized static spherically symmetric $f(T)$ field equations. Their goal was to model anisotropic compact stellar objects by means of a class-one embedding technique. Sossich and Ilijic [75] employed a polytropic EoS within the framework of extended $f(T)$ gravity to construct highly consistent models of compact stars for self-gravitating, non-rotating, and spherically symmetric configurations. Within a theoretical framework based on the torsion scalar, Abbas et al. [76−78] constructed physically realistic models describing anisotropic compact stars by employing diverse fluid configurations. In addition, both this formalism and extended versions of $f(T)$ gravity

CPC Accepted

have been used to study numerous types of ultra-compact astrophysical systems, including pulsars, boson stars, quark stars, neutron stars, strange stars, and wormholes, with the aim of determining their distinctive characteristics and consistency with observations [79−96].

In contrast to models that rely on dark matter, torsion gravity has been shown to offer a viable description of both galactic and large-scale cosmic structures. Li and colleagues [97] provided systematic results to clarify teleparallel gravity using the effective field theory technique. Furthermore, the constraints on gravitational-wave propagation derived from the events *GRB*170817*A* and *GW*170817 have previously established the viability of this approach through effective field theory, especially when specific operators incorporating torsional contributions are employed, as required by observational evidence [98]. From the perspective of this effective approach, Yan and colleagues [99] explored the H_0 and σ_8 discrepancies within extended teleparallel gravity under the Λ-CDM paradigm. The features and physical consequences of gravitational waves in modified $f(T)$ gravity were examined in a review by Farrugia et al. [100]. To ensure clarity, the authors employed a perturbative approach around a Minkowski background that includes a cosmological constant, using both the metric and tetrad fields. To align their results with standard observations, Bahamonde and his collaborators [101] used first-order perturbation theory in torsion gravity, adopting both Schwarzschild and Minkowski backgrounds. From this analysis, they obtained various observational quantities, including photon sphere characteristics and perihelion advance. Bamba and associates [102] examined the impact of trace anomaly on inflation in minimal massive bigravity and quadratic teleparallel $f(T)$ gravity by considering the FLRW universe. Further research on gravitational waves in the context of $f(T)$ theories has been motivated by new observational data from compact binaries in recent works [103,104].

Initially, a self-gravitating fluid with spherical symmetry was assumed to have a perfect matter distribution, meaning that the pressure was equal in all directions. According to the groundbreaking work of Jeans [105], the fluid must be anisotropic because many factors affect the interior geometry. Theoretically, Ruderman [106] found that stellar candidates with densities $> 10^{15}\, g/cm^3$ may not have radial pressure equal to the tangential component. Canuto [107] observed that anisotropy results from differences between radial and transverse pressures because of the significantly increased density of compact stars. Strong magnetic fields [108−111], pion condensation [112], nuclear interactions [107], superfluid cores [113], and other factors can all contribute to anisotropy inside compact objects. After examining how anisotropy affects the equilibrium of celestial configurations, Bowers and Liang [114] concluded that this factor could not be neglected in the core. This factor significantly affects stellar mass, surface redshift, and equilibrium conditions. Using a specific anisotropic factor and radial metric function, Sharif and Naseer [115] derived anisotropic solutions and found that their results were consistent with physical conditions.

In several studies of compact stellar modeling, spacetime geometries described by two metric functions are commonly treated by adopting suitable ansatzes for both metric functions or by fixing one geometric functional form and using the commonly applied class-one Karmarkar condition to determine the remaining spacetime function, thereby obtaining tractable solutions of the equations of motion. This methodology frequently incorporates the *EoS* [116−118] or imposes restrictions on the matter components, such as pressure isotropy [119]. Recently, the complexity-free condition has also gained considerable attention, as proposed in [120]. In contrast, the current investigation applies a different methodology by specifying only the radial geometric function through the Finch–Skea solution, $e^{\alpha(r)} = 1 + sr^2$, while deriving the temporal metric function $\beta(r)$ through the integration of the extended field equations in conjunction with the phenomenological MIT Bag model. This technique establishes a direct link between the spacetime geometry and the underlying matter distribution, thereby reducing the need for additional choices regarding the metric functions. The principal novelty of this study lies in developing a self-consistent analytical model of anisotropic strange quark stars within the linear $f(\mathfrak{T})$ gravity framework by employing this geometric and matter-sector prescription. The resulting solutions are then analyzed in terms of their regularity, boundary matching, physical admissibility, and stability. In addition, the model is applied to the compact stars SAX J1808.4−3658 and 4U 1608−52 to examine the implications of the adopted framework for their structural attributes. This approach provides a systematic means of exploring the interplay between the extended field equations, the Bag model *EoS*, and the resulting stellar structure.

Our paper is organized as follows: In Section **II**, we outline the fundamental concepts of teleparallel gravity and define the essential forms required to develop the theory. Next, by varying the action, we obtain the field equations in $f(T)$ gravity. In Section **III**, we solve these field equations using the Finch-Skea spacetime together with the MIT Bag model. Subsequently, we ensure continuity between the star's external Schwarzschild spacetime and its interior line element. Sections **IV** and **V** present the physical analysis and stability of our model, respectively. These sections investigate a range of the star's physical attributes, such as its density distribution, internal pressures, radial derivatives, pressure anisotropy, adiabatic indices, and sound speed, for different choices of the parameters. These characteristics are presented graphically.

CPC Accepted

Furthermore, we include numerical values in a table for key model parameters, such as central density and central pressure. In Section **VI**, we present the structural evolutionary properties to further support the regularity and physical consistency of our model. Finally, the main results of our study are summarized in Section **VII**.

II. MODEL OF STATIC RELATIVISTIC INTERIOR SPACETIME IN $f(T)$ FORMALISM

For the specified matter distribution, the alternative gravitational theory is formulated from the action given by [121,122]

$$S = \int d^4x e\left[\tfrac{1}{2k^2} f(\mathfrak{T}) + \mathcal{L}_{\rm m}\right]. \tag{1}$$

In natural (geometrized) units, where $G = c = 1$, the function $f(\mathfrak{T}) = f$ depends on the torsion scalar $\mathfrak{T}$, while $\mathcal{L}_{\rm m}$ denotes the Lagrangian density of the matter field. We consider the general line element of a manifold

$$ds^2 = g_{\phi\varphi}\, dx^{\phi} d^{\varphi} = \eta_{ab}\, h^a{}_{\phi}\, h^b{}_{\varphi}\, dx^{\phi} dx^{\varphi}, \tag{2}$$

where

$$\eta_{ab} = \mathrm{diag}(1,-1,-1,-1), \quad dx^{\phi} = e^{\phi}{}_a h^a, \quad h^a = e^a{}_{\phi} dx^{\phi}.$$

Here, Greek indices denote spacetime coordinates, whereas Latin indices label the tetrad field. The determinant of the tetrad is $e = \sqrt{-g} = \det(e^a{}_{\phi})$. When the Riemann tensor is non-vanishing and torsion is present, the Weitzenböck connection is expressed as

$$\Gamma^{\gamma}{}_{\phi\varphi} = e^{\gamma}_a \partial_{\phi} e^a{}_{\varphi}. \tag{3}$$

The torsion tensor is defined as

$$\mathfrak{T}^{\gamma}{}_{\phi\varphi} = \Gamma^{\gamma}{}_{\phi\varphi} - \Gamma^{\gamma}{}_{\varphi\phi} = e^{\gamma}{}_a\left(\partial_{\phi} e^a{}_{\varphi} - \partial_{\varphi} e^a{}_{\phi}\right), \tag{4}$$

whereas the contorsion tensor is given by

$$K^{\gamma}{}_{\phi\varphi} = -\frac{1}{2}\left(\mathfrak{T}_{\phi}{}^{\gamma}{}_{\varphi} - \mathfrak{T}_{\varphi}{}^{\gamma}{}_{\phi} - \mathfrak{T}^{\gamma}{}_{\phi\varphi}\right). \tag{5}$$

Using Eqs. (4) and (5), the superpotential tensor can be expressed as

$$S_{\gamma}{}^{\phi\varphi} = \frac{1}{2}\left(\delta^{\phi}_{\gamma}\mathfrak{T}^{\alpha\varphi}{}_{\alpha} + K^{\phi\varphi}{}_{\gamma} - \delta^{\varphi}_{\gamma}\mathfrak{T}^{\alpha\phi}{}_{\alpha}\right). \tag{6}$$

The required form of the torsion scalar is therefore given by

$$\mathfrak{T} = \mathfrak{T}^{\gamma}{}_{\phi\varphi} S_{\gamma}{}^{\phi\varphi}. \tag{7}$$

Consequently, the equations of motion for $f(\mathfrak{T})$ gravity are obtained by varying the action (1) with respect to the tetrads, yielding the following:

$$\begin{aligned} &e^{-1}\partial_{\alpha}\left(e\, e^{\gamma}{}_{\phi} S_{\gamma}{}^{\alpha\varphi}\right) f_{\mathfrak{T}} + e^{\gamma}{}_{\phi} S_{\gamma}{}^{\alpha\varphi}\, \partial_{\alpha}\mathfrak{T}\, f_{\mathfrak{T}\mathfrak{T}} \\ &+ e^{\alpha}{}_{\phi}\mathfrak{T}^{\tau}{}_{\alpha\beta} S_{\tau}{}^{\varphi\beta} f_{\mathfrak{T}} - \frac{1}{4} e^{\varphi}{}_{\phi} f = -4\pi e^{\tau}{}_{\phi}\left(T^{\varphi}{}_{\tau}\right). \end{aligned} \tag{8}$$

The Lagrangian density $\mathcal{L}_m$ of the matter field is characterized by the stress-energy-momentum tensor T^{φ}_{τ}, while the functional derivatives $f_{\mathfrak{T}}$ and $f_{\mathfrak{T}\mathfrak{T}}$ are defined as $\frac{\partial f}{\partial \mathfrak{T}}$ and $\frac{\partial^2 f}{\partial \mathfrak{T}^2}$, respectively. In the present analysis, an anisotropic fluid distribution is assumed within the stellar interior, such that the pressure is not limited to the radial component P_r but also includes the tangential component P_t. This configuration, governed by pressure anisotropy, is particularly suitable for examining the physical properties of compact astrophysical objects, especially those exhibiting a significant degree of anisotropic behavior. Consequently, the stress-energy-momentum tensor for an anisotropic matter distribution is expressed as follows:

$$T_{\phi\varphi} = \left(\rho + P_t\right) W_{\phi} W_{\varphi} - P_t g_{\phi\varphi} + \left(P_r - P_t\right)\psi_{\phi}\psi_{\varphi}. \tag{9}$$

The matter variables ρ, P_r, and P_t denote the energy density, radial pressure, and tangential pressure, respectively. Furthermore, W^{ϕ} denotes the fluid four-velocity, whereas ψ^{ϕ} corresponds to the spacelike radial unit vector. With these definitions, the gravitational field equations in the extended teleparallel framework can be reformulated in an equivalent Einstein tensor form as follows:

$$\mathcal{G}^{\varphi}_{\phi} = \tfrac{8\pi}{f_{\mathfrak{T}}}\left(T^{\varphi(m)}_{\phi} + T^{\varphi(\mathfrak{T})}_{\phi}\right), \tag{10}$$

where

$$T^{\varphi(m)}_{\phi} = diag(\rho, -P_r, -P_t, -P_t), \tag{11}$$

and

$$T^{\varphi(\mathfrak{T})}_{\phi} = \frac{1}{8\pi}\left[\frac{\mathfrak{T} f_{\mathfrak{T}} - f}{2}\delta^{\varphi}_{\phi} - f_{\mathfrak{T}\mathfrak{T}} S^{\beta\tau}_{\phi}\delta^{\varphi}_{\beta}\delta^{\tau}_{\tau}\Delta_{\tau}\mathfrak{T}\right], \tag{12}$$

CPC Accepted

is a tensor that incorporates additional contributions from the torsion scalar through the modified terms. To investigate the internal structure, we consider a spherically symmetric, static spacetime metric expressed by the following line element:

$$\mathrm{ds}^2 = -e^{\alpha}\mathrm{dr}^2 - r^2\mathrm{d}\theta^2 - r^2\sin^2\theta\,\mathrm{d}\phi^2 + e^{\beta(r)}\mathrm{dt}^2. \tag{13}$$

The metric potentials α and β are taken to be functions of the radial coordinate, denoted by $\alpha(r)$ and $\beta(r)$, respectively. The explicit solutions for the spacetime variables, derived within the framework of a matter–geometry coupled model and presented in the subsequent section, are used to examine the analytical structure of the $f(\mathfrak{T})$ field equations in a more concise form. The tetrad matrix corresponding to the line element in Eq. (13) is given by

$$\left[e_{\phi}^{\varphi}\right] = diag\left[e^{\frac{\beta}{2}}, e^{\frac{\alpha}{2}}, r, r\sin\theta\right]. \tag{14}$$

Alternatively, the determinant of the tetrad matrix can be written as $e = \det\left[e_{\phi}^{\varphi}\right] = e^{\frac{\beta+\alpha}{2}} r^2 \sin\theta$, and the torsion scalar and its derivative are obtained as follows:

$$\mathfrak{T}(r) = \frac{2e^{-\alpha}}{r^2}\left(r\beta' + 1\right), \tag{15}$$

$$\mathfrak{T}'(r) = \frac{2e^{-\alpha}}{r}\left[\beta'' - \frac{1}{r^2} - \left(\beta' + \frac{1}{r}\right)\left(\alpha' + \frac{1}{r}\right)\right]. \tag{16}$$

It is appropriate to clarify the behavior of $\mathfrak{T}$ in the Minkowski limit. For $\alpha = \beta = 0$, the metric reduces to Minkowski spacetime expressed in spherical coordinates. However, substituting these values into Eq. (15) yields $\mathfrak{T}(r) = 2/r^2$, which is nonzero. This result arises from the diagonal tetrad with a vanishing spin connection used in the present analysis and reflects the inertial contributions associated with this tetrad choice in spherical coordinates. In the covariant formulation of teleparallel $f(\mathfrak{T})$ gravity, the relevant inertial spin connection is included together with the tetrad to account for these inertial contributions. Consequently, the torsion scalar for the corresponding Minkowski tetrad-spin connection pair vanishes. Thus, the nonzero value obtained from Eq. (15) should be understood as a consequence of the chosen tetrad-spin connection configuration rather than as evidence of nontrivial gravitational curvature in Minkowski spacetime. The set of $f(\mathfrak{T})$ field equations governing the anisotropic and spherically symmetric interior spacetime model is given as follows:

$$\left[\frac{1}{r^2} - e^{-\alpha}\left(\frac{1}{r^2} - \frac{\alpha'}{r}\right)\right] = \frac{8\pi}{f_{\mathfrak{T}}}\left[\rho + \frac{1}{8\pi}\left\{\frac{\mathfrak{T}\mathfrak{f}_{\mathfrak{T}} - \mathfrak{f}}{2} - f_{\mathfrak{T}\mathfrak{T}}\frac{e^{-\alpha}}{2}\left(\frac{\beta'}{2} + \frac{1}{r}\right)\mathfrak{T}'\right\}\right], \tag{17}$$

$$\left[\frac{1}{r^2} - e^{-\alpha}\left(\frac{1}{r^2} + \frac{\beta'}{r}\right)\right] = \frac{8\pi}{f_{\mathfrak{T}}}\left[-P_r + \frac{1}{8\pi}\left\{\frac{\mathfrak{T}\mathfrak{f}_{\mathfrak{T}} - \mathfrak{f}}{2}\right\}\right], \tag{18}$$

$$-\frac{e^{-\alpha}}{2}\left[\beta'' + \frac{\beta'^2}{2} - \frac{\alpha'\beta'}{2} + \frac{\beta'}{r} - \frac{\alpha'}{r}\right] = \frac{8\pi}{f_{\mathfrak{T}}}\left[-P_t + \frac{1}{8\pi}\left\{\frac{\mathfrak{T}\mathfrak{f}_{\mathfrak{T}} - \mathfrak{f}}{2} - \mathfrak{T}' f_{\mathfrak{T}\mathfrak{T}}\frac{e^{-\alpha}}{2}\left(\frac{\beta'}{2} + \frac{1}{r}\right)\right\}\right]. \tag{19}$$

It is evident from Eqs. (17)–(19) that the preceding system reduces to the corresponding equations of motion in *GR* when $f(\mathfrak{T}) = \mathfrak{T}$. By contrast, $f(\mathfrak{T})$ gravity yields an additional off-diagonal field equation, expressed as follows:

$$\frac{\cot\theta}{2r^2}\mathfrak{T}' f_{\mathfrak{T}\mathfrak{T}} = 0. \tag{20}$$

It is crucial to note that the constraint $\mathfrak{T}' f_{\mathfrak{T}\mathfrak{T}} = 0$, obtained from the non-diagonal equation in $f(\mathfrak{T})$ gravity, is derived for the diagonal tetrad with a vanishing spin connection adopted in the present investigation. Accordingly, this condition is associated with the specific tetrad–spin-connection configuration and should not be regarded as a universal restriction in all formulations of $f(\mathfrak{T})$ gravity. In the covariant formulation, the tetrad and the corresponding inertial spin connection must be considered together, and the resulting field equations may differ from those obtained using a vanishing spin connection. Within the present framework, the non-diagonal equation admits two branches: either $\mathfrak{T}$ is constant, $\mathfrak{T}' = 0$, or the second derivative of the gravitational function vanishes, $f_{\mathfrak{T}\mathfrak{T}} = 0$. In this work, we adopt the latter branch, which leads to a linear functional form within torsion-based gravity.

$$f(\mathfrak{T}) = \lambda_1\mathfrak{T} + \lambda_2. \tag{21}$$

The subsequent analysis is therefore restricted to this specific model and the tetrad-spin connection configuration, while the parameters λ_1 and λ_2 arise as constants of integration. For this linear functional $f(\mathfrak{T})$ model, the second derivative of the Lagrangian vanishes, i.e., $f_{TT} = 0$. Since the teleparallel torsion scalar and the scalar curvature differ by a total-divergence term, the linear

CPC Accepted

torsion action is dynamically equivalent to the Einstein–Hilbert action of *GR*, up to a boundary contribution. The parameter λ_1 modifies the effective gravitational coupling, while the term λ_2 acts as a cosmological-constant-like contribution. Consequently, the present model does not describe genuinely nonlinear torsion contributions in $f(\mathfrak{T})$ gravity. Rather, it provides a linear torsional formulation equivalent to *GR* with effective gravitational parameters, coupled to an anisotropic fluid satisfying the MIT Bag *EoS*. The resulting stellar configurations should therefore be understood as analytical solutions within this effective gravitational framework, rather than as configurations that cannot be interpreted within *GR*.

It is important to clarify the physical interpretation of the adopted linear model $f(\mathfrak{T})=\lambda_1\mathfrak{T}+\lambda_2$. Since $f_{\mathfrak{TT}}=0$, the model does not contain nonlinear modifications of teleparallel gravity and is dynamically equivalent to the teleparallel equivalent of *GR*, with effective gravitational parameters. Thus, the present framework should not be interpreted as introducing genuinely new gravitational dynamics beyond the corresponding *GR* description. Instead, the parameters λ_1 and λ_2 rescale the effective gravitational coupling and the constant geometric contribution entering the stellar field equations. Their impact on the resulting stellar configurations is analyzed in conjunction with the chosen Finch–Skea ansatz and MIT Bag *EoS*. Accordingly, the physical properties obtained in this work are interpreted within this effective *GR*-equivalent framework, and no additional effects associated with nonlinear torsion dynamics are claimed.

Alternatively, one may consider the condition $\mathfrak{T}'=0$ instead of $f_{\mathfrak{TT}}=0$, leading to an extended $f(\mathfrak{T})$ framework with a constant torsion scalar ($\mathfrak{T}=\mathfrak{T}_0$). However, this choice lacks a clear physical interpretation in the context of realistic relativistic stellar solutions [123]. In fact, it can be inferred from Eq. (18) that, as $r\to 0$, the right-hand side of the equation diverges for constant torsion, implying an unphysical blow-up in the pressure. Consequently, this scenario is not physically viable and is therefore excluded from further consideration. By substituting Eq. (21) into Eqs. (17)–(19), we obtain the corresponding gravitational field equations within the modified $f(\mathfrak{T})$ framework.

$$8\pi\rho=\lambda_1\left[\frac{1}{r^2}-e^{-\alpha}\left(\frac{1}{r^2}-\frac{\alpha'}{r}\right)\right]+\frac{\lambda_2}{2}, \tag{22}$$

$$8\pi P_r=\lambda_1\left[\frac{-1}{r^2}+e^{-\alpha}\left(\frac{1}{r^2}+\frac{\beta'}{r}\right)\right]-\frac{\lambda_2}{2}, \tag{23}$$

$$8\pi P_t=\lambda_1\left[\frac{e^{-\alpha}}{2}\left(\beta''+\left(\frac{1}{r}+\frac{\beta'}{2}\right)\left(\beta'-\alpha'\right)\right)\right]-\frac{\lambda_2}{2}. \tag{24}$$

In this section, we adopt a matter–geometry coupling approach to derive the exact form of the spacetime variables. This framework provides a tractable mathematical scheme for investigating the structure and evolution of astrophysical compact star models, particularly in cases where alternative geometrical methods are comparatively less straightforward to implement.

III. CONSTRUCTION OF ANISOTROPIC SOLUTIONS IN FINCH-SKEA SPACETIME WITH MIT BAG *EoS*

The primary objective of this study is to construct a physically realistic and stable interior configuration for relativistic compact stars, particularly in regimes where the microphysical nature and interactions of the constituent particles remain uncertain. This objective can be achieved by deriving analytical solutions to the governing field equations that consistently describe static, spherically symmetric, and highly dense stellar systems. However, obtaining exact solutions is challenging because of the inherent nonlinearity of the coupled second-order differential equations. To address this difficulty, several approaches have been developed to reduce the system to a more tractable form, thereby enabling physically meaningful solutions. Since matter and geometry are intrinsically coupled in the gravitational field equations, we adopt a matter–geometry approach to simplify the analysis. In this context, a well-motivated choice of one of the metric potentials is employed as a seed ansatz, from which the remaining spacetime functions can be constructed consistently. In particular, we consider the Finch–Skea ansatz, originally proposed in [124] for static, spherically symmetric stellar configurations. Although an earlier attempt was made by Duorah and Ray [125], it did not provide a sufficiently robust formulation to fully satisfy the Einstein field equations for realistic stellar modeling. By contrast, the Finch–Skea geometry has demonstrated strong phenomenological relevance in the description of isotropic perfect-fluid spheres, producing solutions that satisfy regularity and physical viability conditions [126]. Extensive studies have also shown that this ansatz maintains consistency and physical admissibility across a wide range of stellar models with different matter sources [127−131]. Moreover, it has been successfully applied to derive astrophysical and cosmological implications within *GR* and its extended theories, with results that remain compatible with observational data [132−150]. Motivated by these features, we adopt the Finch–Skea spacetime and consider the corresponding metric component g_{rr} as the initial seed solution, as given in [124].

CPC Accepted

$$e^{\alpha} = 1 + sr^2. \tag{25}$$

In addition, we introduce a phenomenological linear MIT Bag model as the matter profile [151−154], which effectively captures the essential features of strange quark matter in compact objects composed of deconfined quarks. In this context, Jasim et al. [155] reported significant results using the MIT Bag model by adopting a constant parameter value of $\frac{7}{25}$, corresponding to massive strange quarks with a mass of 250 MeV [156]. However, many studies commonly use a value of $\frac{1}{3}$ to describe massless strange quarks; this choice is adopted in the present analysis to model strange quark configurations. It is well established that a compact stellar object composed of strange quark matter can remain in stable equilibrium when the Bag constant B_g is approximately 60 $MeVfm^{-3}$ [152]. Accordingly, the linear MIT Bag model for the anisotropic matter distribution is expressed as follows:

$$P_r = \frac{1}{3}\left(\rho - 4B_g\right). \tag{26}$$

By employing the Finch–Skea ansatz together with the phenomenological MIT bag equation of state (EoS) (26) in Eqs. (22-24), we obtain the final form of the extended gravitational field equations governing viable stellar configurations.

$$\rho = \frac{1}{8\pi}\left[\frac{\left(r^2 s+3\right)\lambda_1 s}{\left(r^2 s+1\right)^2} + \frac{\lambda_2}{2}\right], \tag{27}$$

$$P_r = \frac{1}{3}\left[\frac{1}{8\pi}\left\{\frac{\left(r^2 s+3\right)\lambda_1 s}{\left(r^2 s+1\right)^2} + \frac{\lambda_2}{2}\right\} - 4B_g\right], \tag{28}$$

$$\begin{aligned} P_t = \frac{1}{144\pi\lambda_1\left(r^2 s+1\right)^3}\Big[&512\pi^2 B_g^2 r^2\left(r^2 s+1\right)^4 + 32\pi B_g\left(r^2 s+1\right)^2\left(-2\lambda_2\left(r^3 s+r\right)^2 - \lambda_1\left(r^2 s\left(4r^2 s+15\right)+6\times\right)\right) \\ &+ 2\lambda_1^2 s\left(r^2 s\left(2r^2 s\left(2r^2 s+9\right)+15\right)+9\right) + \lambda_1\lambda_2\left(r^2 s\left(8r^2 s+21\right)+3\right)\left(r^2 s+1\right)^2 + 2\lambda_2^2 r^2\left(r^2 s+1\right)^4\times\Big], \end{aligned} \tag{29}$$

with

$$\beta = \frac{2}{3}\left[r^2 s - \frac{\left(16\pi B_g - \lambda_2\right)\left(r^2 s+1\right)^2}{4\lambda_1 s} + \frac{1}{2}\log\left(r^2 s+1\right)\right] + A. \tag{30}$$

The adoption of the MIT Bag model within the torsion-based gravitational framework warrants further clarification, as its use here is not merely an ad hoc continuation of earlier implementations but is physically motivated by its ability to capture the essential features of deconfined quark matter while remaining sufficiently tractable under extended $f(\mathfrak{T})$ corrections. In torsion-driven gravity, the effective matter variables receive additional geometric contributions from the torsion scalar, which can obscure the direct interpretation of more complicated equations of state. In this context, the linear MIT Bag EoS provides a minimal yet physically consistent representation of quark matter, in which the Bag parameter B_g encapsulates the non-perturbative vacuum energy effects predicted by Quantum Chromodynamics within a single constant. This simplicity is advantageous for distinguishing genuine gravitational effects from underlying microphysical uncertainties. Moreover, the linear form preserves a transparent relationship between pressure and energy density, making it possible to trace how torsional modifications influence the stiffness and stability of the system without introducing additional complexity. Therefore, its implementation within the $f(\mathfrak{T})$ formalism is justified not by convention alone but by its effectiveness as a controlled framework through which the impact of modified gravity can be consistently examined and physically interpreted.

A. Matching Conditions

The matching conditions are a fundamental geometrical requirement for consistently joining two spacetime regions across a boundary hypersurface ($r \overset{\Sigma}{=} \tilde{\mathcal{R}}$), ensuring both physical continuity and mathematical compatibility. In particular, this smooth matching connects the interior spacetime to an appropriate exterior solution at the junction interface and allows the unknown constants required to establish the model's regularity and physical viability to be determined. Since the underlying field equations are formulated within a torsion-based framework and de-

CPC Accepted

scribe a static, spherically symmetric configuration, the exterior region is chosen to be the standard Schwarzschild spacetime [157], which remains physically consistent and well justified under these assumptions. Accordingly, the exterior metric can be written as follows

$$\mathrm{ds}^2 = -\left(1-\frac{2\tilde{\mathcal{M}}}{r}\right)^{-1} dr^2 - r^2 d\theta^2 - r^2 \sin^2\theta d\phi^2 + \left(1-\frac{2\tilde{\mathcal{M}}}{r}\right) dt^2. \tag{31}$$

Here, $\tilde{\mathcal{M}}$ denotes the total mass of the stellar configuration. The impact of torsion-induced corrections on the gravitational field equations is reflected in the imposed boundary conditions, which ensure the continuity of the metric functions and their derivatives through the first fundamental form, as well as the smooth matching of the extrinsic curvature across the stellar surface. This guarantees a consistent transition between the interior and exterior geometries within the framework of $f(\mathfrak{T})$ gravity. At the boundary hypersurface $r \overset{\Sigma}{=} \tilde{\mathcal{R}}$, the intrinsic spacetime satisfies the first fundamental conditions, namely $g_{tt}^{-} = g_{tt}^{+}$, $g_{rr}^{-} = g_{rr}^{+}$, and $\frac{\partial g_{tt}^{-}}{\partial r} = \frac{\partial g_{tt}^{+}}{\partial r}$, thereby ensuring continuity. These conditions lead to the following expressions

$$e^{\beta(\tilde{\mathcal{R}})} = \left(1-\frac{2\tilde{\mathcal{M}}}{\tilde{\mathcal{R}}}\right), \tag{32}$$

$$e^{-\alpha(\tilde{\mathcal{R}})} = \left(1-\frac{2\tilde{\mathcal{M}}}{\tilde{\mathcal{R}}}\right), \tag{33}$$

$$\frac{2\tilde{\mathcal{M}}}{\tilde{\mathcal{R}}^2} = \frac{2}{3}\left(1-\frac{2\tilde{\mathcal{M}}}{\tilde{\mathcal{R}}}\right) \times \left(2\tilde{R}s + \frac{\tilde{R}s}{1+\tilde{R}^2 s} - \frac{\tilde{R}\left(1+\tilde{R}^2 s\right)\left(16\pi B_g - \lambda_2\right)}{\lambda_1}\right). \tag{34}$$

The second fundamental form requires continuity of the extrinsic curvature across the boundary, which yields $P_r(\tilde{\mathcal{R}}) = 0$ and leads to the following:

$$\frac{1}{3}\left[\frac{1}{8\pi}\left\{\frac{\left(r^2 s+3\right)\lambda_1 s}{\left(r^2 s+1\right)^2} + \frac{\lambda_2}{2}\right\} - 4B_g\right] = 0. \tag{35}$$

Thus, explicitly solving the above expressions yields the model parameter values, which can be written in the following forms.

$$s = \frac{2\tilde{\mathcal{M}}}{\tilde{\mathcal{R}}^2\left(\tilde{R}-2\tilde{\mathcal{M}}\right)}, \tag{36}$$

$$A = \log\left(1-\frac{2\tilde{\mathcal{M}}}{\tilde{\mathcal{R}}}\right) - \frac{2}{3}\left(\tilde{R}^2 s - \frac{\left(1+\tilde{R}^2 s\right)^2\left(16\pi B_g - \lambda_2\right)}{4s\lambda_1} + \frac{1}{2}\log\left(1+\tilde{R}^2 s\right)\right), \tag{37}$$

$$B_g = \frac{1}{16\pi}\left(\frac{\left(-2\tilde{\mathcal{R}}^4 s^2\left(\tilde{R}-2\tilde{\mathcal{M}}\right) - 3\tilde{\mathcal{R}}^2 s\left(\tilde{\mathcal{R}}-3\tilde{\mathcal{M}}\right) + 3\tilde{\mathcal{M}}\right)\lambda_1}{\left(2\tilde{\mathcal{M}}-\tilde{\mathcal{R}}\right)\left(\tilde{\mathcal{R}}^3 s+\tilde{\mathcal{R}}\right)^2} + \lambda_2\right), \tag{38}$$

$$\tilde{\mathcal{R}} = \sqrt{\frac{\sqrt{\lambda_1 s^3\left(256\pi B_g - 4\lambda_2 + \lambda_1 s\right)} + s\left(-64\pi B_g + \lambda_2 + \lambda_1 s\right)}{s^2\left(64\pi B_g - \lambda_2\right)}}. \tag{39}$$

The solutions for the unknown parameters are expressed in terms of the mass and radius, consistent with observational data for compact objects. Within this modified $f(\mathfrak{T})$ framework, an explicit solution for estimating the stellar radius is also presented. These solutions are expected to play a significant role in revealing novel structural and evolutionary features of compact star models, particularly through the effective contribution of torsion-like terms. To support the analysis, we consider observational data for two well-known compact star candidates, namely $SAXJ1808.4-3658$ and $4U1608-52$, treating them as representative test cases for examining astrophysical compact geometries that may serve as alternatives to strange quark stars. It should be noted that the parameter s has units of km^{-2}, A is a dimensionless constant, and λ_2 is fixed at $0.0001 km^{-2}$ throughout the analysis.

Notably, a non-zero λ_2 introduces a constant geometric term into the gravitational field equations, which formally acts as a cosmological constant. In a fully consistent treatment, the exterior vacuum solution should

CPC Accepted

Table 1. The numerically evaluated values of the unknown constant s and the corresponding compactness are presented based on observational data for various viable compact star models.

Compact Stars	$\tilde{\mathcal{R}}(km)$	$\tilde{\mathcal{M}}(M_\odot)$	$\tilde{\mathcal{M}}\,(Km)$	$\frac{\tilde{\mathcal{M}}}{\tilde{\mathcal{R}}}$	$s\ (km^{-2})$
$SAXJ1808.4-3658$	7.07	1.435	2.116625	0.299381	0.029854790
$4U1608-52$	9.3	1.74	2.5665	0.275967	0.014242357
$CenX-3$	9.17	1.49	2.19775	0.239667	0.010948175
$PSRJ1614-2230$	9.69	1.97	2.90575	0.299871	0.015957942

therefore be the Schwarzschild-de Sitter or Schwarzschild-anti-de Sitter metric, depending on the sign of λ_2. However, the physical relevance of this term must be assessed in relation to the characteristic scales of the problem under consideration. The value adopted in our analysis is $\lambda_2 = 0.0001\,km^{-2}$. To place this in perspective, for a typical compact star with radius $R \sim 10\,km$, the surface curvature scale is of order $1/R^2 \sim 10^{-2}\,km^{-2}$, which is two orders of magnitude larger than λ_2. More importantly, the dimensionless contribution of the cosmological-constant-like term at the stellar surface is of order $\lambda_2 R^2 \sim 0.0001 \times 100 = 0.01$, corresponding to at most a 1% correction to the metric function. In practice, compared with the dominant gravitational term $2M/R \sim 0.3$-0.4 for the compact stars considered, the λ_2-induced correction is suppressed by a factor of $\sim 10^{-4}$ relative to the leading-order Schwarzschild term. Consequently, the exterior spacetime is effectively Schwarzschild to an excellent approximation, and including a cosmological horizon term would introduce additional mathematical complexity. Furthermore, the linear $f(\mathfrak{T})$ model (21) considered here is dynamically equivalent to *GR* with an effective gravitational coupling λ_1 and a constant term λ_2. In the teleparallel formulation, the vacuum field equations with a linear torsion scalar admit the same spherically symmetric solutions as *GR*, with the λ_2 term appearing as an effective cosmological constant. For stellar-mass compact objects, this term is negligible at the boundary, and the Schwarzschild metric provides an accurate and physically consistent exterior description. We have therefore employed the Schwarzschild exterior (31) as an excellent approximation, with the matching conditions imposed at the stellar boundary, where the λ_2-induced corrections are suppressed by a factor of $\sim 10^{-4}$ relative to the dominant gravitational terms.

IV. CREDIBILITY OF $f(\mathfrak{T})$-BASED SOLUTIONS USING THERMODYNAMIC PROPERTIES

To establish the essential physical criteria, we examine the thermodynamic quantities that underpin the robustness of the derived solutions within the extended $f(\mathfrak{T})$ field equations. These quantities provide physical and theoretical support for the consistency of the spacetime model in describing relativistic compact stellar configurations within a modified gravity framework. In particular, the thermodynamic variables–identified with the matter components–play a fundamental role in characterizing any realistic fluid distribution. Their analysis enables an assessment of the physical viability and credibility of the stellar interior by ensuring the regular behavior of the geometric functions, the consistency of the Bag constant, and the feasibility of the matter variables and their gradients. Furthermore, the evaluation of the state parameters and the fulfillment of the energy conditions contribute to validating the model. A series of graphical analyses is employed to illustrate these features, provide clear insight into the underlying behavior, and strengthen the physical interpretation of the proposed spacetime configuration within torsion-based gravity.

A. Physical concordance of geometric solutions

We examine the physical consistency and coherence of the metric functions used to construct a viable model of strange quark stars, with particular emphasis on obtaining realistic spacetime solutions compatible with stellar interior configurations. To ensure viability, the geometric functions must satisfy essential conditions: they should remain regular at the stellar center and finite and positive throughout the interior region of the fluid distribution. In this context, the metric potentials satisfy the central conditions $e^{\beta(0)} = e^{\frac{6A\lambda_1 s - 16\pi B_g + \lambda_2}{6\lambda_1 s}}$ and $e^{\alpha(0)} = 1$. Furthermore, the corresponding derivatives of the metric functions are expressed as follows:

$$\frac{de^{\alpha}}{dr} = 2sr, \tag{40}$$

$$\begin{aligned}\frac{de^{\beta}}{dr} = \frac{2}{3}\Bigg(&- \frac{r\left(16\pi B_g - \lambda_2\right)\left(r^2 s+1\right)}{\lambda_1} + \frac{rs}{r^2 s+1} + 2rs\Bigg) \\ &\times \exp\Bigg(A + \frac{2}{3}\Bigg(- \frac{\left(16\pi B_g - \lambda_2\right)\left(r^2 s+1\right)^2}{4\lambda_1 s} \\ &+ r^2 s + \frac{1}{2}\times \log\left(r^2 s+1\right)\Bigg)\Bigg).\end{aligned} \tag{41}$$

CPC Accepted

● We examine the physical behavior of the spacetime solutions in the interior and exterior regions for two distinct compact star candidates, as illustrated in Fig. 1. In both regions, the solutions exhibit regular, well-behaved profiles, with no singularity at the stellar center, and remain finite and positive throughout the fluid sphere. The interior and exterior solutions are also smoothly matched at the junction interface (see both plots), which supports the physical viability and consistency of the proposed geometric model within this alternative theory of gravity. Consequently, the results provide a reliable and coherent description of the stellar interior structure of compact objects.

B. Quantification of Bag parameter B_g

Within the context of $f(\mathfrak{T})$ gravity, in which torsion-driven contributions modify the effective gravitational interaction, the MIT Bag *EoS* acquires enhanced physical relevance because of its sensitivity to geometry–matter coupling. In this framework, the bag constant B_g is not merely a fixed QCD parameter but is effectively constrained by the extended field equations.

● In assessing the impact of the Bag parameter on the possible formation of astrophysical compact objects, particularly in relation to strange quark interactions, we observe a physically consistent and well-behaved trend. The parameter remains positive throughout the entire distribution for different choices of λ_1 (see Fig. 2). Both profiles show that the Bag parameter evolves systematically with varying parameter values, as indicated by the dotted curves. This increasing trend is more pronounced in the first model than in the second, and both models attain their maximum values at the highest considered λ_1. The ranges obtained for the Bag parameter span 63.41 $MeVfm^{-3}$ to 170.53 $MeVfm^{-3}$ and 34.88 $MeVfm^{-3}$ to 94.90 $MeVfm^{-3}$ for the proposed models $SAXJ1808.4-3658$ and $4U1608-52$, respectively, as also summarized in Tables 2–3. Notably, the first model consistently satisfies the approximate benchmark value of 60 $MeVfm^{-3}$ reported in [152] for all choices of λ_1,

CPC Accepted

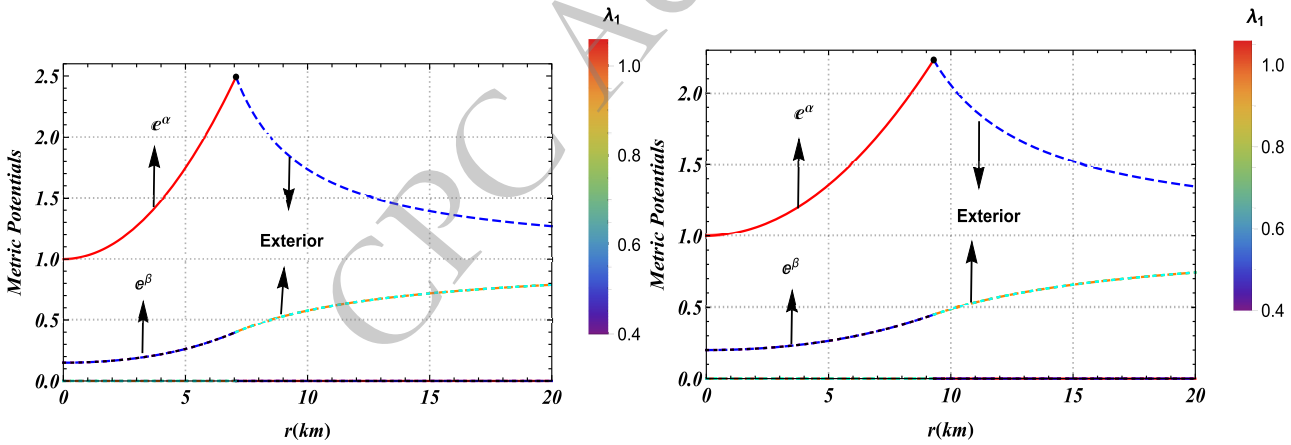

Fig. 1. (color online) Consistency and regularity of the geometric solutions across the interior and exterior spacetimes as functions of the radial coordinate r for two well-known compact-star candidates, $SAXJ1808.4-3658$ (left panel) and $4U1608-52$ (right panel).

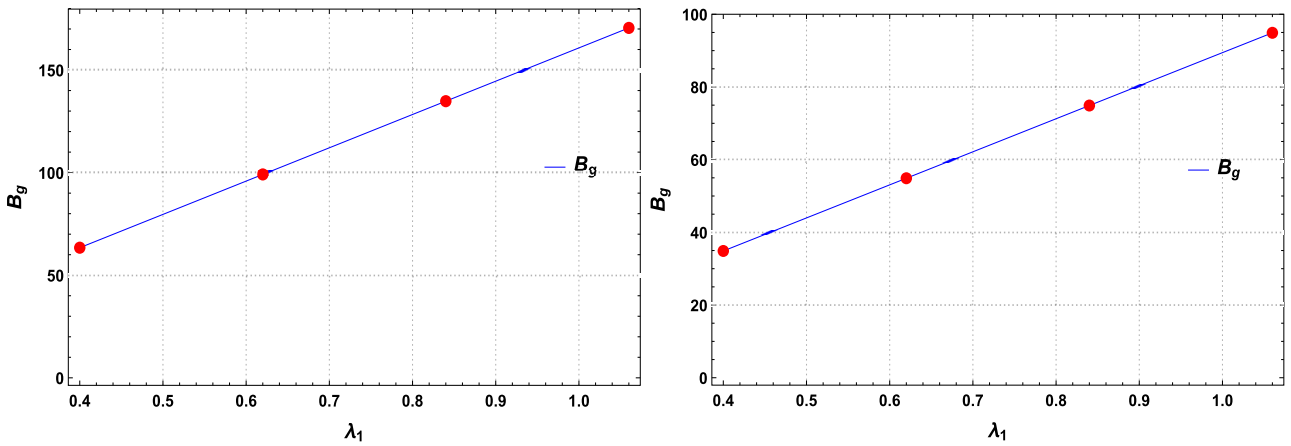

Fig. 2. (color online) Variation of the bag constant B_g as a function of the theoretical parameter λ_1, illustrating its role in the potential formation of the compact objects $SAXJ1808.4-3658$ and $4U1608-52$.

Table 2. The numerically estimated values are presented in tabular form for various choices of the theory parameter λ_1. These values include the unknown constant A, the bag constant B_g, and the matter variables evaluated at the stellar center and surface. In addition, the adiabatic index and its critical value, together with the predicted radius, mass, compactness, and redshift parameters, are reported for the representative compact object $SAXJ1808.4-3658$.

λ_1	A	$B_g\ (MeVfm^{-3})$	$\rho(0)\ (\frac{g}{cm^3})$	$\rho(s)\ (\frac{g}{cm^3})$	$P_r(0)\ (\frac{dyne}{cm^2})$	Γ	Γ_{cric}	$\tilde{\mathcal{R}}\ (km)$ from the model	$\tilde{\mathcal{M}}\ (Km)$ from the model	$\frac{\tilde{\mathcal{M}}}{\tilde{\mathcal{R}}}$	$\frac{2\tilde{\mathcal{M}}}{\tilde{\mathcal{R}}}$	Z_s
0.4	−1.838103858	63.41	1.9207×10^{15}	4.6100×10^{14}	4.4033×10^{35}	1.642	1.441	7.14	0.844	0.119	0.238	0.146
0.62	−1.838103943	99.12	2.9786×10^{15}	7.1603×10^{14}	6.8119×10^{35}	1.645	1.501	7.11	1.309	0.185	0.370	0.260
0.84	−1.838103776	134.82	4.0365×10^{15}	9.7105×10^{14}	9.2204×10^{35}	1.647	1.560	7.10	1.775	0.251	0.502	0.417
1.06	−1.838103678	170.53	5.0944×10^{15}	1.2261×10^{15}	1.1629×10^{36}	1.648	1.620	7.09	2.241	0.317	0.634	0.653

Table 3. The numerically evaluated values of the unknown constant A, the Bag constant B_g, and the matter variables at the stellar center and surface are presented in tabular form. In addition, the adiabatic index and its critical value, together with the predicted radius, mass, compactness, and redshift, are reported for different choices of the parameter λ_1 for the well-known compact star model $4U1608-52$.

λ_1	A	$B_g\ (MeVfm^{-3})$	$\rho(0)\ (\frac{g}{cm^3})$	$\rho(s)\ (\frac{g}{cm^3})$	$P_r(0)\ (\frac{dyne}{cm^2})$	Γ	Γ_{cric}	$\tilde{\mathcal{R}}\ (km)$ from the model	$\tilde{\mathcal{M}}\ (Km)$ from the model	$\frac{\tilde{\mathcal{M}}}{\tilde{\mathcal{R}}}$	$\frac{2\tilde{\mathcal{M}}}{\tilde{\mathcal{R}}}$	Z_s
0.4	−1.53898278	34.88	9.1489×10^{14}	2.5717×10^{14}	1.9973×10^{35}	1.708	1.433	9.48	1.020	0.110	0.220	0.132
0.62	−1.53898746	54.89	1.4196×10^{15}	4.0009×10^{14}	3.0826×10^{35}	1.715	1.487	9.42	1.585	0.170	0.340	0.232
0.84	−1.53898620	74.89	1.9242×10^{15}	5.4301×10^{14}	4.1678×10^{35}	1.718	1.542	9.39	2.149	0.231	0.462	0.364
1.06	−1.53898546	94.90	2.4288×10^{15}	6.8593×10^{14}	5.2530×10^{35}	1.720	1.597	9.37	2.714	0.292	0.584	0.550

CPC Accepted

whereas the second model satisfies this condition only for the two largest values of λ_1, indicating a more restricted regime for the realization of strange quark matter configurations.

The range obtained in this work may represent a notable improvement over previous studies, which typically report narrower or less consistent intervals within standard gravity. This broader yet admissible domain indicates that torsional contributions in $f(\mathfrak{T})$ gravity provide additional flexibility in regulating the stiffness of quark matter, allowing both softer and stiffer configurations to coexist without violating stability or energy conditions. Consequently, the present model not only aligns more closely with the expected QCD bounds but also demonstrates that $f(\mathfrak{T})$-induced corrections can substantially extend the physically viable parameter space of compact star candidates, offering a more consistent and realistic description than previously developed approaches.

C. Physical evaluation of matter variables

The key matter variables–energy density and radial and tangential pressures–constitute the fundamental components of the fluid distribution and play a central role in determining the structural stability and physical viability of compact stellar systems. Accordingly, we examine the model solutions by analyzing these physically relevant quantities and incorporating the properties of strange quark matter under the influence of the torsion-based gravity parameter.

● Figure 3 illustrates the effect of variations in the energy density on the formation of static and spherically symmetric compact star candidates for different choices of the torsional parameter λ_1. The energy density in both plots exhibits non-negative and regular behavior, preserving the essential non-singularity at every interior point of the compact stellar distribution. In both profiles, this physical quantity reaches its maximum near the central core, indicating that the interior composition is well suited to high-density regimes, a typical feature of ultra-compact objects [106,158,159]. It then gradually decreases toward the boundary surface as the radial distance r increases, but it does not vanish. This feasible behavior is also evident from the numerically estimated values presented in Tables 2 and 3, where the central values remain greater than those at the boundary, consistent with the graphical results and supporting the potential coherence of our model solutions. These collective features support the physical adequacy and acceptability of our extended gravity solutions for describing celestial objects whose interiors are composed of strange quark matter.

● We examine the influence of the radial and tangential pressure terms on the strange quark matter distribution associated with the formation of a stable interior stellar structure for astrophysical compact objects in Figs. 4-

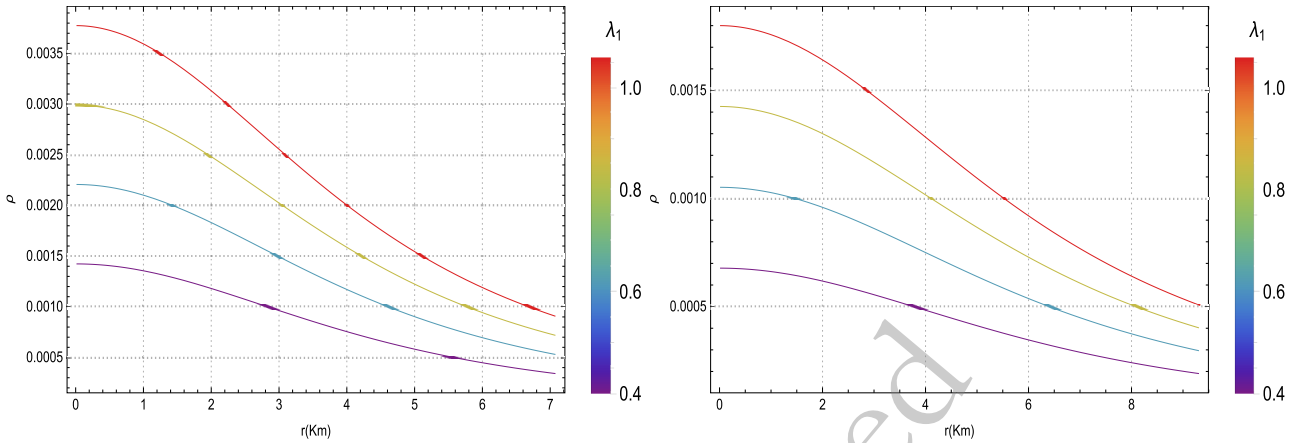

Fig. 3. (color online) Variation of the energy density with r for the spherically symmetric compact-star models $SAXJ1808.4-3658$ and $4U1608-52$.

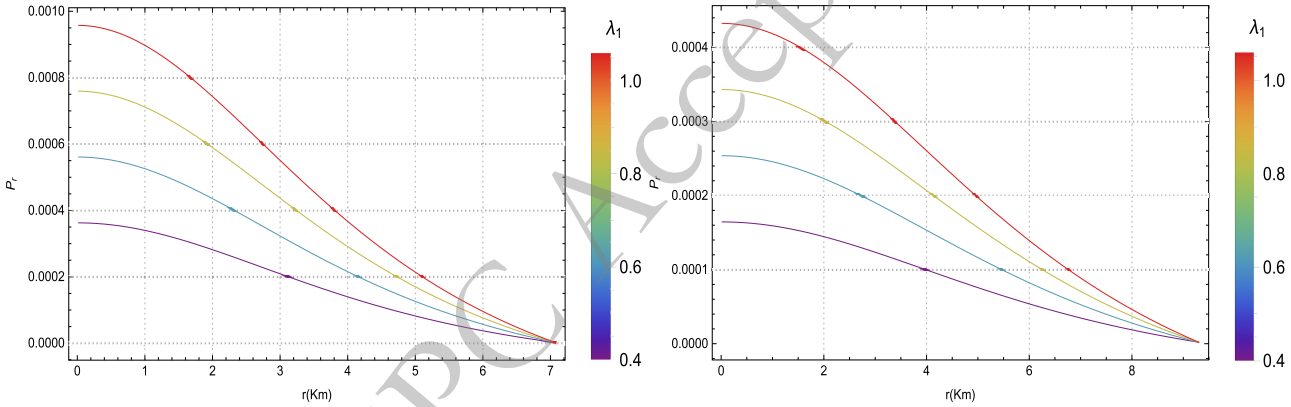

Fig. 4. (color online) Variation of radial pressure as a function of the radial coordinate r for two prominent compact star candidates, $SAXJ1808.4-3658$ and $4U1608-52$.

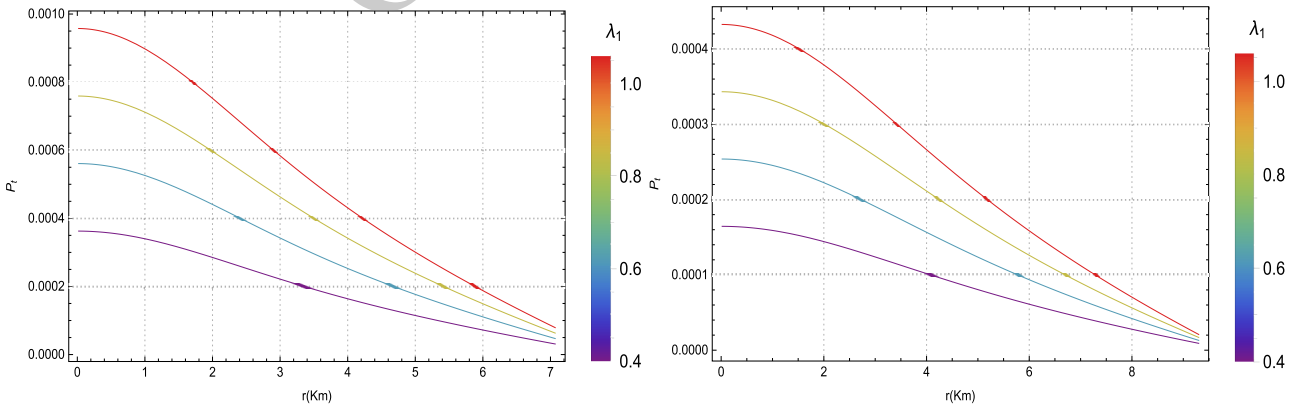

Fig. 5. (color online) Profiles of tangential pressure as a function of the radial coordinate r for the static spheroidal models $SAXJ1808.4-3658$ and $4U1608-52$.

5. These pressure quantities exhibit well-behaved profiles and remain positive and regular, without producing any singularities at interior points throughout the fluid distribution. In particular, the radial pressure decreases rapidly and vanishes at the surface, while attaining its maximum value near the central region (see Fig. 4). In contrast, the transverse pressure does not vanish at the boundary surface, which primarily reflects the spheroidal nature of strange quark stars (see Fig. 5). It consistently exhibits regularity and a well-defined trend, thereby supporting the viability of a stable interior configuration. Moreover, the numerical values of the radial pressure at the center are presented in Tables 2–3; these values further show good agreement with standard theoretical es-

CPC Accepted

timates and significantly enhance the reliability of our results within the underlying gravity framework. The corresponding analytical solutions for these matter quantities at the center are given as follows:

$$\rho(0)=\frac{\lambda_2+6\lambda_1 s}{16\pi}, \tag{42}$$

$$P_r(0)=P_t(0)=\frac{-64\pi B_g+\lambda_2+6\lambda_1 s}{48\pi}. \tag{43}$$

● We examine the physical acceptability of the proposed spacetime solutions by analyzing the radial gradients of the prescribed matter variables in Fig. 6. The behavior of these gradient functions throughout the distribution shows that they are physically consistent, remaining negative and bounded at every interior point of the fluid spheres. Thus, the necessary conditions $\frac{d\rho}{dr}\le 0$, $\frac{dP_r}{dr}\le 0$, $\frac{dP_t}{dr}\le 0$ are satisfied without violating the required limits. This behavior is consistent with theoretical expectations for interior relativistic configurations, in which negative radial gradients are essential for maintaining sufficient pressure support against gravitational collapse. Overall, these features further confirm the viability of our model solutions for describing stable interior stellar structures composed of strange quark matter.

D. Equation of state

The most commonly used form, frequently adopted by theorists, is the standard EoS, defined as $P_\phi=\omega_\phi\rho$, which describes the primary matter distribution within the stellar interiors of compact celestial objects. This parameter reflects the effects of the underlying matter content, either indicating regions of instability or supporting an internally stabilized and physically realistic spacetime configuration. Since the present model is constructed as a static, anisotropic, and spherically symmetric strange quark star distribution, the corresponding solutions for the state parameters are as follows

$$\omega_r=\frac{1}{3\left(6\lambda_1 s(r^2s+3)+3\lambda_2(r^2s+1)^2\right)}\left[-192\pi B_g\left(r^2s+1\right)^2+6\lambda_1 s\left(r^2s+3\right)+3\lambda_2\left(r^2s+1\right)^2\right], \tag{44}$$

$$\begin{aligned}\omega_t=&\frac{1}{9\lambda_1(r^2s+1)\left(2\lambda_1 s(r^2s+3)+\lambda_2(r^2s+1)^2\right)}\left[512\pi^2B_g^2r^2\left(r^2s+1\right)^4+32\pi B_g\left(r^2s+1\right)^2\left(-2\lambda_2\left(r^3s+r\right)^2\right.\right.\\&\left.-\lambda_1\left(4r^4s^2+15r^2s+6\right)\right)+2\lambda_1^2 s\left(r^2s\left(2r^2s\left(2r^2s+9\right)+15\right)+9\right)+\lambda_1\lambda_2\left(r^2s\left(8r^2s+21\right)+3\right)\left(r^2s+1\right)^2\\&\left.+2\lambda_2^2r^2\left(r^2s+1\right)^4\right].\end{aligned} \tag{45}$$

● We examine the radial variation of the state parameters in both the radial and tangential directions to assess the physical admissibility of strange quark star candidates as functions of the radial distance r in Figs. 7–8. The profiles of both state parameters, along with their magnified views, exhibit finite and consistent behavior,

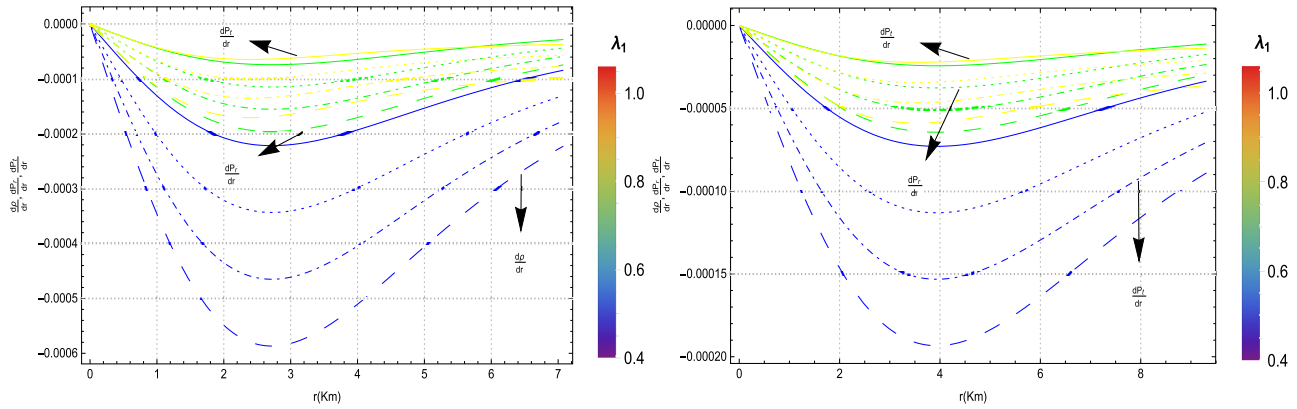

Fig. 6. (color online) The variations of the matter variables, expressed in terms of their first radial gradients with respect to r, are presented for two viable compact star candidates, $SAXJ1808.4-3658$ and $4U1608-52$.

CPC Accepted

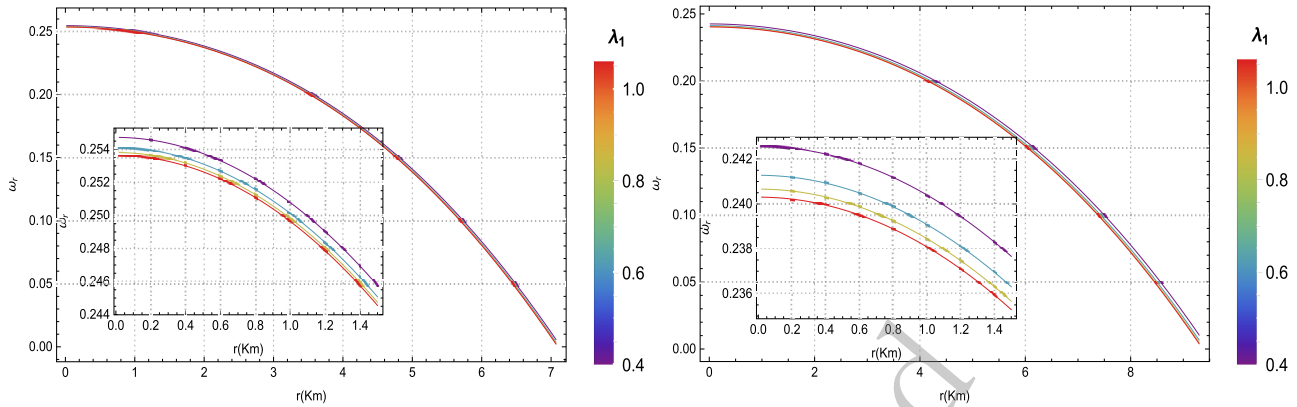

Fig. 7. (color online) Variation in the radial state parameter as a function of the radial coordinate r for the strange quark star candidates $SAXJ1808.4-3658$ and $4U1608-52$.

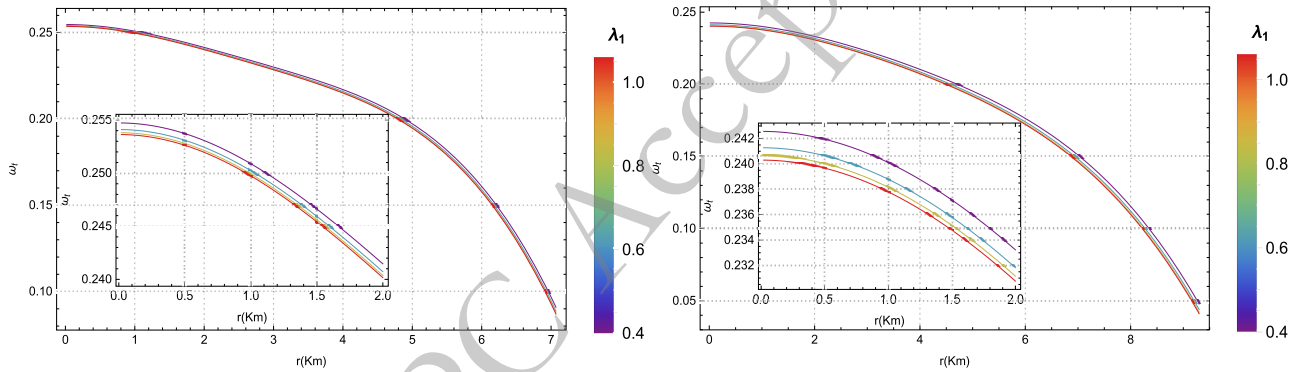

Fig. 8. (color online) Variation in the tangential state parameter as a function of r for two viable compact stellar models, $SAXJ1808.4-3658$ and $4U1608-52$.

CPC Accepted

thereby ensuring regularity and the absence of singularities at all interior points of the compact objects. Their constrained ranges also show that they lie within the physically acceptable interval $[0,1]$, satisfying the standard conditions $0 \le \omega_r \le 1$ and $0 \le \omega_t \le 1$. These features indicate that the spacetime configuration remains in a potentially stable equilibrium state, with no instability regions or exotic behavior that could affect the properties of the principal matter distribution [160].

E. Energy Conditions

Energy bounds on the relationships between the energy density and pressure terms must be imposed to ensure that the spacetime solutions remain physically consistent and capable of describing the internal structural dynamics of astrophysical compact objects. This criterion plays a pivotal role in assessing the fluid distribution through the prescribed matter variables, which may collectively indicate stability or the presence of exotic features within the stellar interior. The necessary and sufficient relations for the energy conditions in the extended $f(\mathfrak{T})$ framework for a spherically symmetric strange quark star configuration are expressed as follows:

$$\begin{aligned}
&\text{WEC}: \ \rho \ge 0, \quad \rho + P_r \ge 0, \quad \rho + P_t \ge 0,\\
&\text{NEC}: \rho + P_r \ge 0, \quad \rho + P_t \ge 0,\\
&\text{DEC}: \ \rho \ge |P_r|, \quad \rho \ge |P_t|,\\
&\text{SEC}: \ \rho + P_r \ge 0, \quad \rho + P_t \ge 0, \quad \rho + P_r + 2P_t \ge 0,\\
&\text{TEC}: \ \rho - P_r - 2P_t \ge 0.
\end{aligned} \tag{46}$$

● In Fig. 9, we analyze the combined influence of different energy bounds on the strange quark matter distribution for two well-known compact objects for various choices of the $f(\mathfrak{T})$ parameter. Each curve corresponding to the energy conditions remains positive, well behaved, and regular at all interior points of the compact object configuration. These conditions are more prominent near the stellar core, where they attain their maximum values, and gradually decrease toward the stellar surface as the radial distance increases. Such features strongly support the tractability and physical adequacy of the spacetime solutions for modeling stable relativistic stellar structures composed of strange quark matter within the framework of this alternative gravity theory.

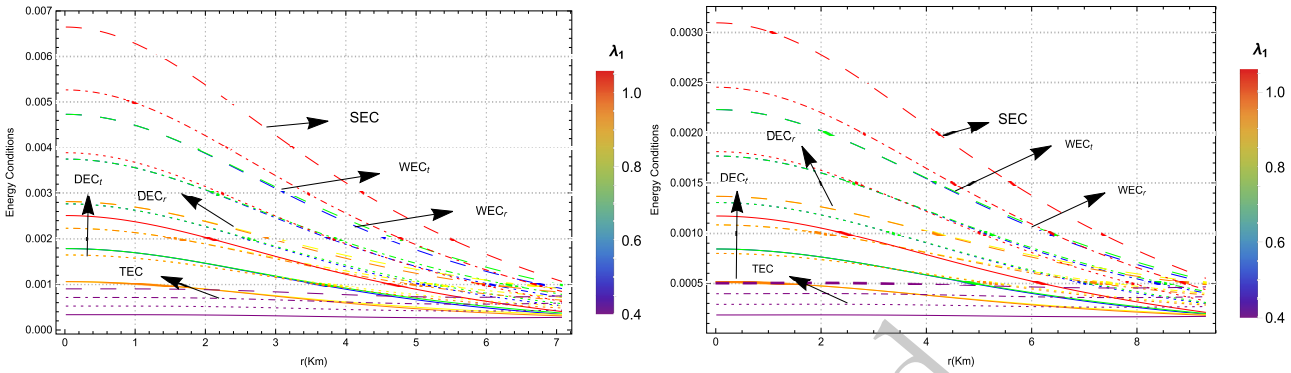

Fig. 9. (color online) Physical interpretation of various energy bounds as functions of the radial distance r for the spheroidal strange quark compact objects $SAXJ1808.4-3658$ and $4U\ 1608-52$.

V. STABILITY ANALYSIS

Notwithstanding the rigorous assessment of torsion-corrected spacetime solutions under various physical constraints, the viability of the $f(\mathfrak{T})$ geometric model must also be examined within another essential framework: stability. Stability constrains the interior dynamics required to preserve the structural integrity of compact stellar systems and establishes a robust parametric domain capable of counteracting instability-driven effects. This criterion encompasses a broad range of physical requirements, including the behavior of anisotropic stress, the validity of Herrera's condition through sound-speed components and the cracking concept, the physical acceptability of force equilibrium, consistency with the relativistic adiabatic index, and the regularity of the static stability condition.

A. Anisotropic stress

An anisotropic stress field is a natural feature of the matter content of relativistic ultra-compact stellar objects, in which pressure acts differently in different directions. By contrast, an isotropic field is characterized by the same pressure in all directions. To investigate the effect of pressure anisotropy on compact stellar interior configurations, it is important to treat anisotropy as a physically realistic phenomenon that may not necessarily affect the stability of stable relativistic ultra-compact interior bodies. For static models, the transverse pressure may or may not vanish at the surface, whereas the radial pressure must vanish identically there. This difference has important consequences for the generation of pressure anisotropy in the interior and determines whether the corresponding anisotropic stress exhibits inward or outward behavior. Hence, for a proposed spacetime model, the exact solution for this anisotropic stress is given by

$$\Delta = P_t - P_r = \frac{1}{72\pi\lambda_1 (r^2 s+1)^3}\Big[r^2\Big(256\pi^2 B_g^2\big(r^2 s+1\big)^4 + 16\pi B_g\big(r^2 s+1\big)^2\Big(-\lambda_1 s\big(4r^2 s+9\big) - 2\lambda_2\big(r^2 s+1\big)^2\Big)$$
$$+\lambda_1^2 s^2\Big(r^2 s\big(4r^2 s+15\big)+3\Big) + \lambda_1\lambda_2 s\big(4r^2 s+9\big)\big(r^2 s+1\big)^2 + \lambda_2^2\big(r^2 s+1\big)^4\Big)\Big]. \tag{47}$$

● In Fig. 10, we examine the role of anisotropic stress in the stability of two distinct compact stars for different values of the torsion parameter λ_1. As shown in both panels, the pressure anisotropy is physically acceptable (positive and regular) throughout the stellar interior and increases from the stellar core to the surface, where it reaches its maximum value. This outward increase helps reinforce the structure of relativistic stellar models, thereby mitigating gravitational instability. Specifically, this behavior indicates that the anisotropic stress is repulsive ($\Delta > 0$) and also implies that the central region of the stellar configuration is dominated by high-density matter [161], which induces substantial pressure anisotropy [162]. The strength and effects of anisotropic stress can therefore serve as indicators of theoretical models of compact stellar objects, including neutron stars and other dense stellar configurations. Thus, the presence of pressure anisotropy further confirms the physical relevance of our model for explaining the stability of strange quark stars in extended $f(\mathfrak{T})$ gravity.

B. Herrera's stability criteria: causality and cracking conditions

Among the various stability criteria, the Herrera caus-

CPC Accepted

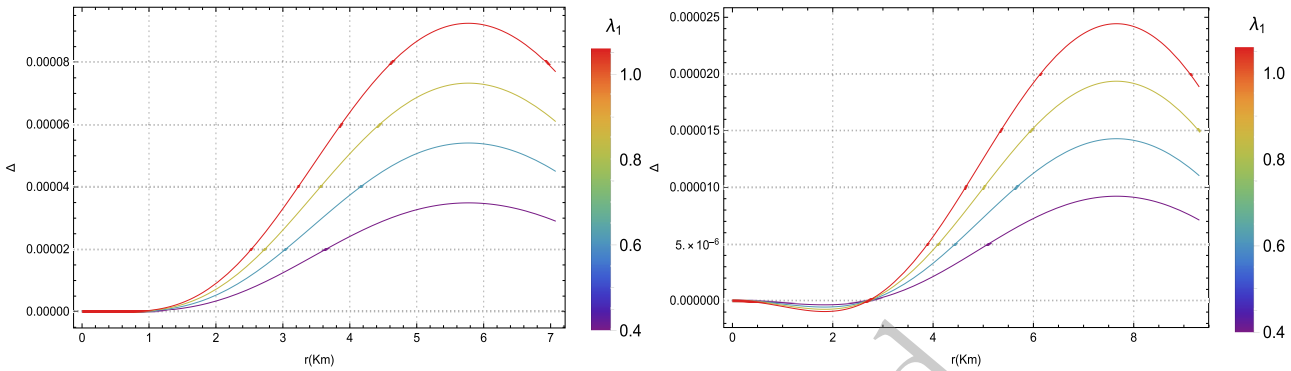

Fig. 10. (color online) Profiles of anisotropic stress as functions of r for the static spheroidal compact stellar geometries $SAXJ1808.4-3658$ and $4U\ 1608-52$.

ality and cracking conditions [163,164] are widely used to assess the stability and physical viability of compact stellar configurations. The causality condition requires the propagation of perturbations within the stellar interior to remain subluminal. In relativistic units ($c=1$), this requirement is expressed in terms of the radial and transverse sound speeds as

$$0 \le v_r^2 = \frac{dp_r}{d\rho} \le 1, \qquad 0 \le v_t^2 = \frac{dp_t}{d\rho} \le 1, \tag{48}$$

which ensure that the matter distribution is physically acceptable and stable against small perturbations [165]. According to the cracking concept proposed by Herrera [166,167], potentially stable regions satisfy $v_r^2 > v_t^2$, whereas potentially unstable regions satisfy $v_t^2 > v_r^2$. Furthermore, the condition

$$\left|v_t^2 - v_r^2\right| \le 1, \tag{49}$$

must be satisfied throughout the stellar interior to prevent cracking and maintain the stability of the compact configuration [164,168]. Thus, the corresponding analytical forms required for the anisotropic spherically symmetric stellar configuration considered here are as follows:

$$v_r^2 = \frac{1}{3}, \tag{50}$$

$$v_t^2 = -\frac{1}{9\lambda_1^2 s^2 (r^2 s+1)(r^2 s+5)}\left[256\pi^2 B_g^2 \left(2r^2 s+1\right)\left(r^2 s+1\right)^4 + 16\pi B_g \left(r^2 s+1\right)^2 \left(-\lambda_1 s\left(4r^2 s\left(r^2 s+2\right)+9\right)\right.\right.$$
$$\left. -2\lambda_2\left(2r^2 s+1\right)\left(r^2 s+1\right)^2\right) - 6\lambda_1^2 s^2\left(r^2 s\left(r^2 s-1\right)+2\right) + \lambda_1\lambda_2 s\left(4r^2 s\left(r^2 s+2\right)+9\right)\left(r^2 s+1\right)^2 + \lambda_2^2\left(2r^2 s\right.$$
$$\left.\left. +1\right)\left(r^2 s+1\right)^4\right], \tag{51}$$

$$S = v_t^2 - v_r^2 = -\frac{1}{27\lambda_1^2 s^2 (r^2 s+1)(r^2 s+5)}\left[3\left(256\pi^2 B_g^2\left(2r^2 s+1\right)\left(r^2 s+1\right)^4 + 16\pi B_g\left(r^2 s+1\right)^2\left(-\lambda_1 s\left(4r^2 s\right.\right.\right.\right.$$
$$\left.\left.\left.\left. \times\left(r^2 s+2\right)+9\right) - 2\lambda_2\left(2r^2 s+1\right)\left(r^2 s+1\right)^2\right) - 6\lambda_1^2 s^2\left(r^2 s\left(r^2 s-1\right)+2\right) + \lambda_1\lambda_2 s\left(4r^2 s\left(r^2 s+2\right)\right.\right.\right.$$
$$\left.\left.\left. +9\right)\left(r^2 s+1\right)^2 + \lambda_2^2\left(2r^2 s+1\right)\left(r^2 s+1\right)^4\right) + 9\lambda_1^2 s^2\left(r^2 s+1\right)\left(r^2 s+5\right)\right]. \tag{52}$$

● The physical behavior associated with the causality and cracking conditions is analyzed in Figs. 11-13. The graphical profiles show that both the radial and transverse sound speeds remain finite and within the allowed

CPC Accepted

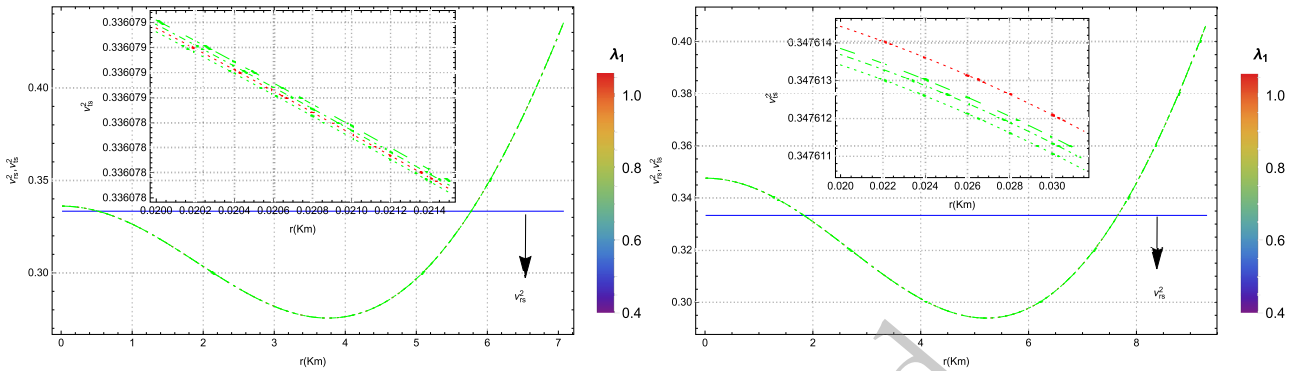

Fig. 11. (color online) Variation of the squared sound-speed components with respect to the radial coordinate r for the two strange quark star candidates $SAXJ1808.4-3658$ and $4U\ 1608-52$.

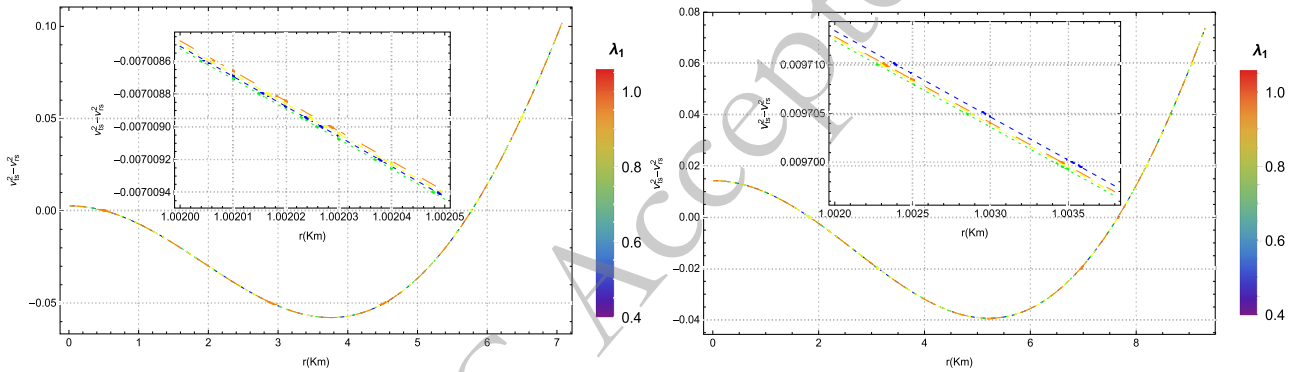

Fig. 12. (color online) Physical analysis of the cracking condition $v_{ts}^2 - v_{rs}^2$ as a function of the radial coordinate r for two viable compact objects, $SAXJ1808.4-3658$ and $4U\ 1608-52$.

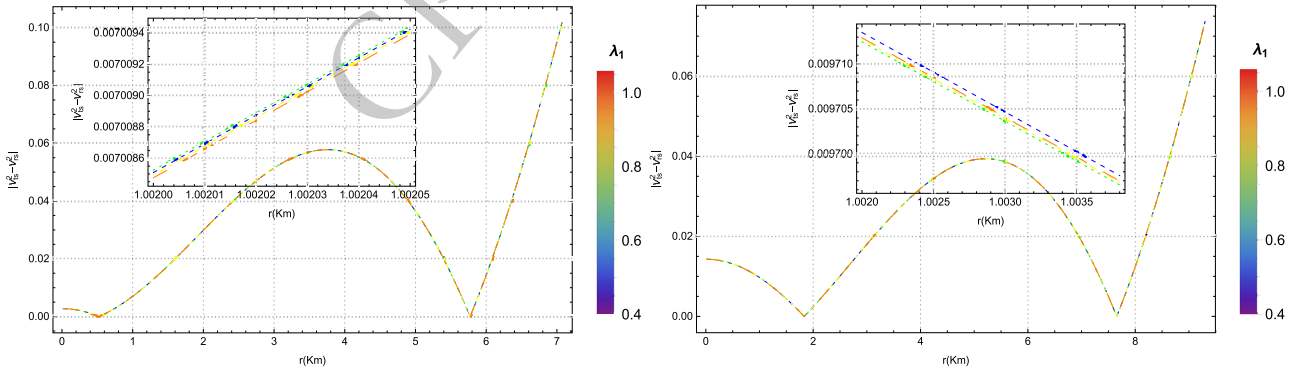

Fig. 13. (color online) Profiles of the cracking condition $|v_{ts}^2 - v_{rs}^2|$ as functions of the radial distance r for the spheroidal compact star geometries $SAXJ1808.4-3658$ and $4U\ 1608-52$.

bounds throughout the stellar interior. Furthermore, the difference between the squared sound speeds satisfies the bound $|v_t^2 - v_r^2| \leq 1$ (see Fig. 13), thereby ensuring physical consistency and regularity at all interior points of the strange quark matter distribution [164]. To assess cracking, we analyze the difference between the squared sound speeds, $S = v_t^2 - v_r^2$, using the condition $v_t^2 - v_r^2 \leq 0$ to examine the absence of cracking in our compact stellar models, as shown in Fig. 12. According to the Abreu-Herrera criterion, $S \leq 0$ indicates a potentially stable region, whereas $S > 0$ corresponds to a potentially cracking-prone region. In particular, the minimum and maximum values of S, together with the corresponding positive-S radial locations, are presented in Table 4. For $SAXJ1808.4-3658$, S takes both negative and positive values, with ranges of $-0.06294 \leq S_{\min} \leq -0.05973$ and $0.09274 \leq S_{\max} \leq 0.09833$ as λ_1 varies from 0.40 to 1.06. For $4U1608-52$, the corresponding ranges are $-0.04946 \leq S_{\min} \leq -0.04317$ and $0.05842 \leq S_{\max} \leq 0.06805$. Thus, positive values of S occur within both stellar configurations, including in an outer region near the surface of each star. These results indicate that the

CPC Accepted

Table 4. Minimum and maximum values of the cracking parameter $S = v_t^2 - v_r^2$ for the two compact-star candidates. The corresponding radial intervals containing these extrema and the regions in which $S > 0$ are also shown.

Compact Stars	λ_1	$S_{\min}$	$r_{\min}$ (km)	$S_{\max}$	$r_{\max}$ (km)	$S > 0$
$SAXJ1808.4-3658$	0.40	−0.06294	3.802	0.09274	7.07	$5.902 < r \le 7.07$
	0.62	−0.06110	3.786	0.09596	7.07	$0 \le r < 0.268$; $5.856 < r \le 7.07$
	0.84	−0.06024	3.778	0.09745	7.07	$0 \le r < 0.350$; $5.834 < r \le 7.07$
	1.06	−0.05973	3.774	0.09833	7.07	$0 \le r < 0.391$; $5.821 < r \le 7.07$
$4U1608-52$	0.40	−0.04946	5.334	0.05842	9.3	$0 \le r < 1.311$; $8.047 < r \le 9.3$
	0.62	−0.04585	5.290	0.06400	9.3	$0 \le r < 1.508$; $7.909 < r \le 9.3$
	0.84	−0.04416	5.269	0.06656	9.3	$0 \le r < 1.595$; $7.844 < r \le 9.3$
	1.06	−0.04317	5.258	0.06805	9.3	$0 \le r < 1.646$; $7.805 < r \le 9.3$

configurations are not free from potentially cracking-prone regions according to the Abreu-Herrera criterion. We therefore conclude that the proposed model satisfies the causality condition and the bound on the absolute difference between the squared sound speeds, whereas the signed difference $v_t^2 - v_r^2$ exhibits regions that do not satisfy the condition associated with the absence of cracking.

C. Hydrostatic equilibrium of forces

In this subsection, we investigate the dynamical stability of the obtained compact star configuration using the Tolman–Oppenheimer–Volkoff (TOV) equation, which describes the hydrostatic equilibrium condition for anisotropic matter distributions. This condition represents the balance among the hydrostatic, gravitational, and anisotropic forces acting within the stellar interior and plays an important role in maintaining the equilibrium of compact stellar systems. In the framework of modified $f(T)$ gravity, the conservation law for a static, spherically symmetric matter distribution is given by $\nabla^a T_{ab} = 0$. Consequently, the corresponding TOV equation takes the form

$$-\frac{dP_r}{dr} - \frac{\beta'\left(\rho + P_r\right)}{2} + \frac{2\left(P_t - P_r\right)}{r} = 0. \tag{53}$$

The preceding equation can be expressed in terms of the hydrostatic force F_h, gravitational force F_g, and anisotropic force F_a as

$$F_h + F_g + F_a = 0, \tag{54}$$

with

$$F_h = -\frac{dP_r}{dr} = -\frac{\lambda_1 r s^2\left(r^2 s + 5\right)}{12\pi\left(r^2 s + 1\right)^3}, \tag{55}$$

$$F_g = -\frac{\beta'\left(\rho + P_r\right)}{2} = -\frac{1}{36\pi\lambda_1\left(r^2 s + 1\right)^3}\left[r\left(16\pi B_g\left(r^2 s + 1\right)^2 - 2\lambda_1 s\left(r^2 s + 3\right) - \lambda_2\left(r^2 s + 1\right)^2\right)\left(16\pi B_g\left(r^2 s + 1\right)^2 - \lambda_1 s\left(2r^2 s + 3\right) - \lambda_2\left(r^2 s + 1\right)^2\right)\right], \tag{56}$$

$$F_a = \frac{2\left(P_t - P_r\right)}{r} = \frac{1}{36\pi\lambda_1\left(r^2 s + 1\right)^3 r}\left[r^2\left(256\pi^2 B_g^2\left(r^2 s + 1\right)^4 + 16\pi B_g\left(r^2 s + 1\right)^2\left(-\lambda_1 s\left(4r^2 s + 9\right) - 2\lambda_2\left(r^2 s + 1\right)^2\right) + \lambda_1^2 s^2\left(r^2 s\left(4r^2 s + 15\right) + 3\right) + \lambda_1\lambda_2 s\left(4r^2 s + 9\right)\left(r^2 s + 1\right)^2 + \lambda_2^2\left(r^2 s + 1\right)^4\right)\right]. \tag{57}$$

● Here, F_h denotes the outward hydrostatic force generated by the pressure gradient, F_g represents the inward gravitational force, and F_a arises from pressure anisotropy within the stellar configuration. The equilibrium

CPC Accepted

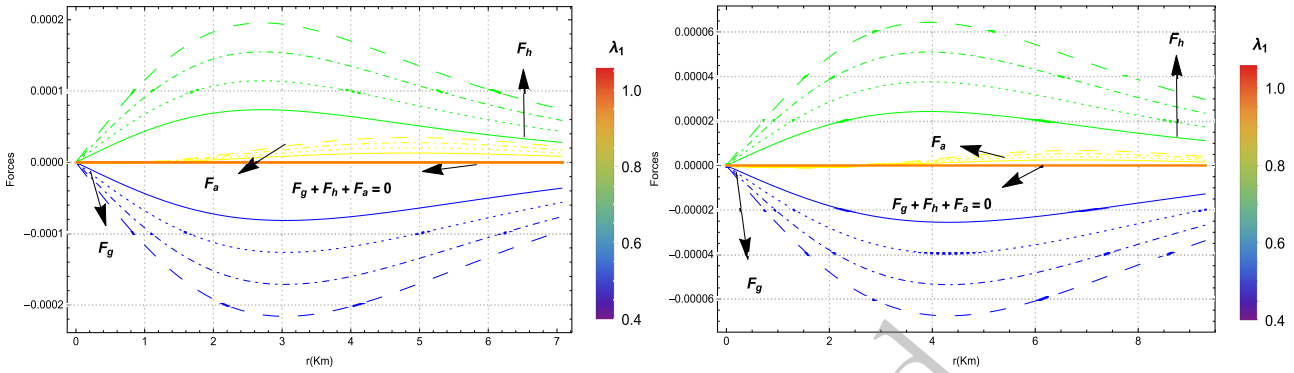

Fig. 14. (color online) Variation in force equilibrium with r for the strange quark star candidates $SAXJ1808.4-3658$ and $4U\ 1608-52$.

condition given in Eq. (54) describes the hydrodynamic balance of the compact object. The behavior of these forces is illustrated in Fig. 14 for different values of the torsion parameter λ_1. All force components remain finite and well behaved throughout the stellar interior. The inward gravitational force is balanced by the combined hydrostatic and anisotropic forces, resulting in a net force equal to zero at each interior point. Therefore, the obtained anisotropic strange quark star configuration satisfies the hydrostatic equilibrium condition and remains physically stable within the framework of modified $f(T)$ gravity.

D. Adiabatic index

To further examine the physical viability and dynamical stability of the resulting stellar configuration, we analyze the relativistic adiabatic index. The response of compact stellar systems to small radial perturbations is crucial for determining their stability, as originally discussed by Chandrasekhar [169]. According to the relativistic stability criterion, a compact stellar configuration remains stable if the adiabatic index satisfies the condition

$$\Gamma > \tfrac{4}{3}. \tag{58}$$

This condition implies that the pressure responds sufficiently to variations in the energy density to counterbalance gravitational attraction and prevent gravitational collapse. Thus, analyzing the adiabatic index is essential for studying the stability and equilibrium behavior of relativistic compact stars.

For a static, spherically symmetric, anisotropic matter distribution, the radial and tangential adiabatic indices are defined as

$$\begin{aligned}\Gamma_r &= \left(\frac{\rho + p_r}{p_r}\right) v_r^2, \\ &= \frac{64\pi B_g \left(r^2 s+1\right)^2 - 8\lambda_1 s\left(r^2 s+3\right) - 4\lambda_2\left(r^2 s+1\right)^2}{64\pi B_g \left(r^2 s+1\right)^2 - 2\lambda_1 s\left(r^2 s+3\right) - \lambda_2\left(r^2 s+1\right)^2} v_r^2,\end{aligned} \tag{59}$$

$$\begin{aligned}\Gamma_t &= \left(\frac{\rho + p_t}{p_t}\right) v_t^2, \\ &= \frac{2}{512\pi^2 B_g^2 r^2 \left(r^2 s+1\right)^4 + 2\lambda_2^2 r^2 \left(r^2 s+1\right)^4 + A_1 + A_2 + A_3} \Big[256\pi^2 B_g^2 r^2 \left(r^2 s+1\right)^4 + 16\pi B_g \left(r^2 s+1\right)^2 \\ &\times \left(-2\lambda_2\left(r^3 s + r\right)^2 - \lambda_1\left(r^2 s\left(4r^2 s+15\right)+6\right)\right) + \lambda_1^2 s\left(r^2 s\left(r^2 s\left(4r^2 s+27\right)+51\right)+36\right) + \lambda_1\lambda_2 \\ &\times \left(r^2 s\left(4r^2 s+15\right)+6\right)\left(r^2 s+1\right)^2 + \lambda_2^2 r^2\left(r^2 s+1\right)^4\Big] v_t^2.\end{aligned} \tag{60}$$

Here

CPC Accepted

$$A_1 = 32\pi B_g\left(r^2 s+1\right)^2\Big(-2\lambda_2\left(r^3 s+r\right)^2 - \lambda_1\left(r^2 s\left(4r^2 s+15\right)+6\right)\Big),$$

$$A_2 = 2\lambda_1^2 s\left(r^2 s\left(2r^2 s\left(2r^2 s+9\right)+15\right)+9\right),$$

$$A_3 = \lambda_1\lambda_2\left(r^2 s\left(8r^2 s+21\right)+3\right)\left(r^2 s+1\right)^2.$$

The corresponding critical value of the relativistic adiabatic index is given by

$$\Gamma_{\rm cri} = \frac{4}{3}+\frac{19U(r)}{21}. \tag{61}$$

● The behavior of the radial and tangential adiabatic indices for the compact star candidates $SAXJ1808.4-3658$ and $4U\ 1608-52$ is shown in Figs. 15–16. Both Γ_r and Γ_t remain positive, finite, and well behaved throughout the stellar interior. Furthermore, the radial and tangential adiabatic indices increase smoothly from the center to the boundary surface and satisfy the stability condition $\Gamma_i > \frac{4}{3}$ $(i=r,t)$ everywhere within the stellar configuration. The numerical values of the adiabatic indices and their critical values are listed in Tables 2–3. These results indicate that the resulting stellar model remains dynamically stable and physically acceptable throughout the interior spacetime. Therefore, the present analysis supports the stability and viability of the proposed anisotropic compact star configuration within the considered gravitational framework.

E. Static stability approach

To examine the static stability of the resulting compact-star configuration, we employ the Harrison-Zel'dovich-Novikov stability criterion [170,171]. According to this criterion, a relativistic stellar configuration remains stable if its total mass increases with central density, i.e.,

$$\frac{dM}{d\rho(0)} > 0. \tag{62}$$

In contrast, the condition $\frac{dM}{d\rho(0)} < 0$ indicates an unstable stellar configuration. For the present compact-star model, the mass as a function of the central density is given by

CPC Accepted

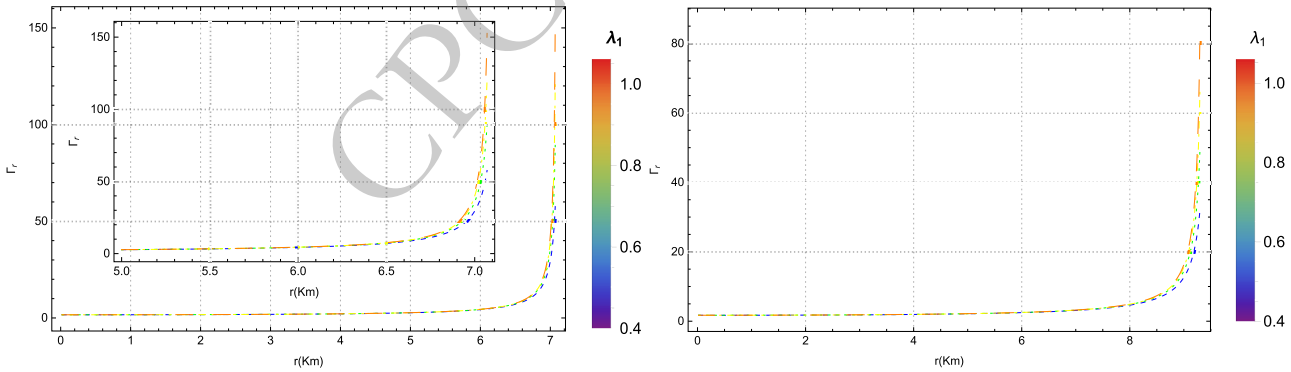

Fig. 15. (color online) Profiles of Γ_r as functions of the radial coordinate r for the two candidate strange quark stars $SAXJ1808.4-3658$ and $4U\ 1608-52$.

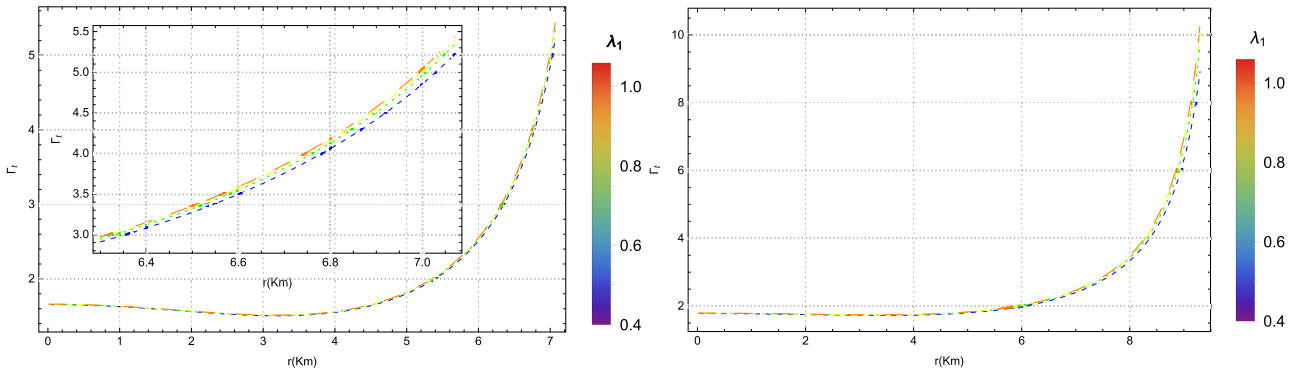

Fig. 16. (color online) Evolution of Γ_t as a function of radial distance r for two viable strange quark star models, $SAXJ1808.4-3658$ and $4U\ 1608-52$.

$$M(\rho(0)) = \frac{\tilde{\mathcal{R}}^3\left(8\pi\rho(0) - \frac{\lambda_2}{2}\right)}{2\left(\tilde{\mathcal{R}}^2\left(8\pi\rho(0) - \frac{\lambda_2}{2}\right) + 3\lambda_1\right)}. \tag{63}$$

Differentiating Eq. (61) with respect to the central density gives

$$\frac{dM}{d\rho(0)} = \frac{48\pi\lambda_1\tilde{\mathcal{R}}^3}{\left(\tilde{\mathcal{R}}^2(\lambda_2 - 16\pi\rho(0)) - 6\lambda_1\right)^2}. \tag{64}$$

- The behavior of the mass–central-density relation, $M(\rho(0))$, and its derivative, $\frac{dM}{d\rho(0)}$, is shown in Figs. 17 and 18 for the compact star candidates $SAXJ1808.4\text{-}3658$ and $4U1608\text{-}52$. To ensure a consistent equilibrium sequence, the central density $\rho(0)$ is varied while the theory parameters are kept fixed, and B_g does not enter the mass–central-density formulation. The resulting $M(\rho(0)) - \rho(0)$ profiles increase monotonically over the considered range of $\rho(0)$ for both compact stellar models. The corresponding derivative remains non-negative along the sequences, indicating that the mass remains regular and finite as the central density varies over the considered range. Thus, the $M(\rho(0))$ analysis is performed along a fixed-parameter equilibrium sequence without simultaneously varying the theory parameters. These results satisfy the Harrison–Zeldovich–Novikov stability criterion and represent physically tractable and consistent stellar configurations.

VI. RELIABILITY OF SOLUTIONS VIA STRUCTURAL ATTRIBUTES

Motivated by the results of our model, which largely establish its physical acceptability and reliability, we now extend our spacetime solutions by incorporating several well-established and physically significant features. Specifically, we examine key structural and evolutionary properties–namely, gravitational mass, compactness, surface redshift, and moment of inertia–which provide important insights into the behavior of relativistic celestial bodies. These quantities must remain nonsingular and regular, and they should vary smoothly with increasing radial distance while preserving internal structural stability and physical consistency. Their analysis has import-

CPC Accepted

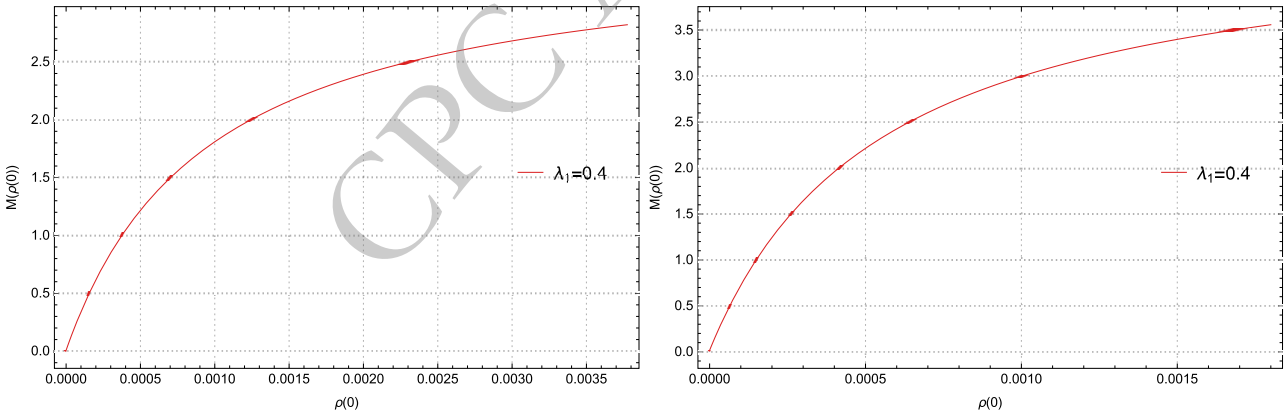

Fig. 17. (color online) Physical implications of the mass function $M(\rho(0))$ versus the central density $\rho(0)$ for two well-known compact stellar objects, $SAXJ1808.4-3658$ and $4U\ 1608-52$.

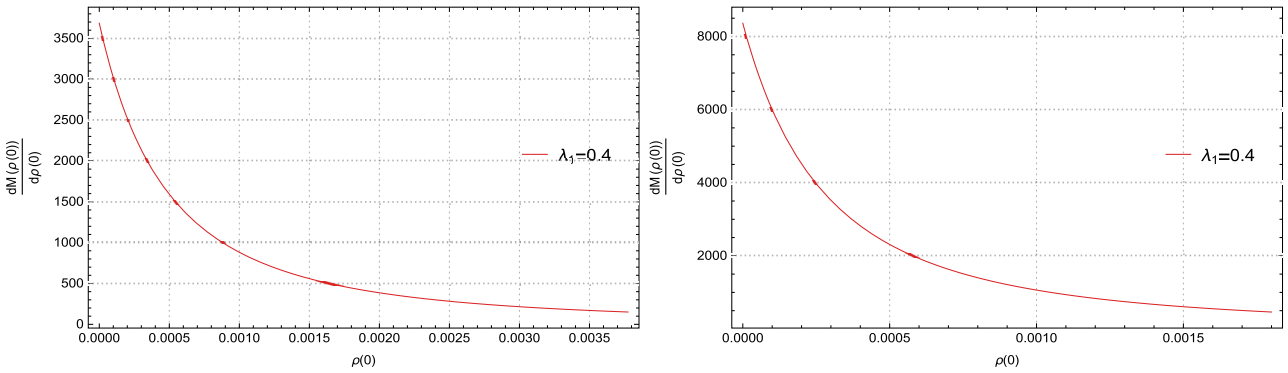

Fig. 18. (color online) Physical implications of the mass-gradient function $\frac{dM}{d\rho(0)}$ with respect to the central density $\rho(0)$ for the spherically symmetric celestial models $SAXJ1808.4-3658$ and $4U\ 1608-52$.

ant implications for the formation of astrophysical compact stars and supports the extraction of physically tractable results from the spacetime configuration. In particular, investigating these parameters establishes a clearer connection with observational data and enables an assessment of whether the proposed stellar models are consistent with, or deviate from, established constraints. Based on such structural characteristics, stellar objects can be classified into different categories, as discussed in previous studies [172]. In this context, we first extend our analysis by determining the mass function from Eq. (27), which represents the total gravitational mass enclosed within a sphere of radius r and is expressed as follows

$$M(r) = 4\pi \int_0^r \rho r^2 dr = r^3 \left(\frac{\lambda_1 s}{2(r^2 s+1)} + \frac{\lambda_2}{12} \right). \quad (65)$$

● We analyze the physical impact of the mass function for two viable strange quark star models corresponding to the various values of the torsion parameter λ_1, as illustrated in Fig. 19. For each value of λ_1, the mass function exhibits a smooth, progressive trend, remains non-negative, and is bounded throughout the entire stellar configuration of the spherically symmetric compact objects. This physical quantity is also observed to increase rapidly from the interior core to the boundary surface as the radial distance increases, reaching its maximum value where $r \sim \tilde{\mathcal{R}}$. These attributes are consistent with the regularity of the spacetime solution and indicate structural consistency in stable, equilibrated strange quark star compact objects.

● More specifically, our study highlights the numerically predicted values for the proposed compact-star model, as listed in Tables **2–3**. Notably, the corresponding magnitudes are quantified as 2.241 and 2.714 at the highest value, $\lambda_1 = 1.06$, for the two testbeds $SAX\,J1808.4-3658$ and $4U1608-52$, respectively. Within this gravity framework, these values exhibit significant concordance with the observed values of these compact objects. This finding is noteworthy because it provides distinct support for the spacetime results within the underlying gravity theory, reflecting its effectiveness without implying that it surpasses the observational results. This consequence also underscores the physical acceptability and potential coherence of the spacetime solutions in modeling ultra-compact stellar structures analogous to neutron stars, as predicted in a previous study [172].

● The mass function derived for the proposed model does not explicitly depend on the Bag constant B_g. The variation in the predicted mass with the effective gravitational coupling parameter λ_1 is determined by the dependence of the mass function on λ_1 and by the fixed values of the remaining model parameters, λ_2 and s. The values of B_g presented in Tables 2 and 3 are included to illustrate the corresponding variation in the Bag constant and the behavior of physical quantities that explicitly depend on it. Thus, the mass predictions and the B_g-dependent consequences should be interpreted according to their respective functional dependencies.

● In addition, we establish the robustness of our spacetime model by showing that the radii predicted from the solution of Eq. (39) are in close agreement with the observed radii of the proposed compact objects listed in Table 1. For both test cases, the predicted radii are reported in Tables 2-3, demonstrating that the model solution is consistent with the observational data within the framework of $f(\mathfrak{T})$ gravitational theory. It is important to clarify that the predicted radius values do not represent the independent influence of λ_1; rather, they are jointly determined by λ_1 and the Bag constant, which is itself controlled by varying λ_1. This dependence of the Bag constant on λ_1 in the radial formulation does not allow the effects of λ_1 to be isolated independently; instead, its influence is collectively reflected through the resulting matter properties.

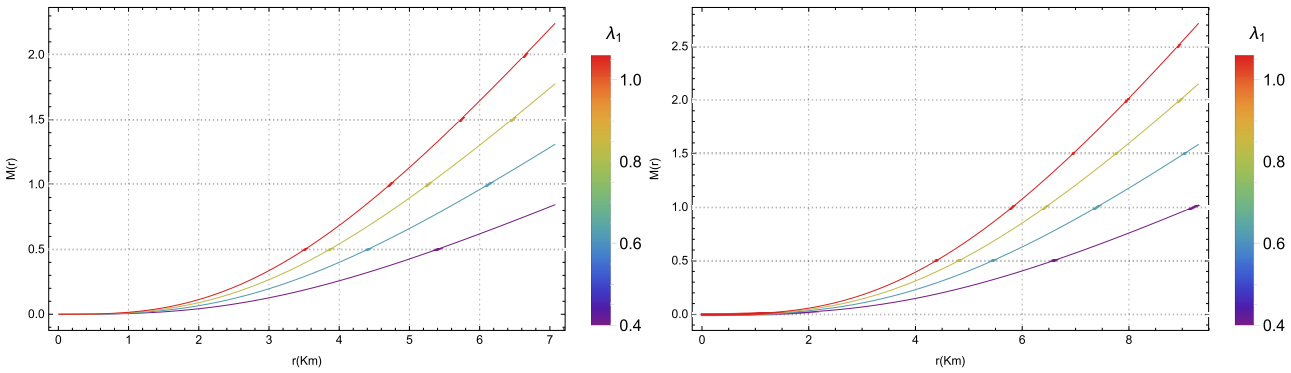

Fig. 19. (color online) Evolution of the mass function with respect to r for the anisotropic spheroidal compact objects $SAXJ1808.4-3658$ and $4U\ 1608-52$.

CPC Accepted

Compactness is quantified by the mass-to-radius ratio, which indicates the strength of gravity and the emergence of relativistic effects in astrophysical compact stellar bodies. A high degree of compactness significantly affects the internal equilibrium state and structural composition of a stellar body, as intense gravitational fields generate substantial spacetime curvature. To analyze the impact of compactness, we examine its physical behavior for the anisotropic and spherically symmetric strange quark matter distribution, which is given by the following analytical solution:

$$U(r)=\frac{M(r)}{r}=r^2\left(\frac{\lambda_1 s}{2(r^2 s+1)}+\frac{\lambda_2}{12}\right). \tag{66}$$

● Figure 20 illustrates the structural evolution of the compactness parameter for two viable strange quark star models under different choices of the torsion parameter λ_1. Both profiles show that the compactness follows a pattern similar to that of the mass function, remains physically acceptable and bounded, and preserves the interior structural consistency and regularity of the compact objects (see Fig. 20). This property also increases rapidly from the stellar center toward the boundary of the compact spheres, where $r\sim\Re$, and attains its maximum values, thereby indicating the structural evolutionary behavior of the compact star models [172].

● Moreover, the maximum compactness values observed in both graphical profiles are further substantiated by the numerical predictions for the considered strange quark star candidates $SAXJ1808.4-3658$ and $4U\ 1608-52$ for different choices of λ_1, as reported in Tables 2–3. Notably, for $\lambda_1=1.06$, these values are predicted to be 0.317 and 0.292, respectively, which are consistent with the graphical behaviors of both compact star models and exceed the corresponding observational values for the compact objects. In addition to this qualitative feature, the compactness satisfies the lower and upper Buchdahl bounds $\frac{M(r)}{r}<\frac{4}{9}$ and $\frac{2M(r)}{r}<\frac{8}{9}$ as proposed in [173]. These characteristic features further support the physical acceptability and viability of our model solutions for describing anisotropic, ultra-dense, stable strange quark stars, thereby providing new insight within the context of $f(\mathfrak{T})$ gravity.

To assess the internal structural stability of the spacetime model, we analyze the redshift parameter for the anisotropic, spherically symmetric distribution, which is given as follows.

$$\begin{aligned}Z_s&=\left(1-2U(r)\right)^{-\frac{1}{2}}-1,\\&=\left(1-2r^2\left(\frac{\lambda_1 s}{2(r^2 s+1)}+\frac{\lambda_2}{12}\right)\right)^{-\frac{1}{2}}-1.\end{aligned} \tag{67}$$

● We examine the impact of the redshift parameter on the structural stability of anisotropic strange quark star models in Fig. 21. In both profiles, the redshift parameter remains non-negative, smooth, and non-singular throughout the stellar interior of the compact objects. It increases monotonically from the stellar center as the radial distance r increases and reaches maximum finite values at the boundary surface (see Fig. 21). Moreover, we corroborate our graphical analysis with the numerically predicted values for the selected star models, as reported in Tables 2-3. These computed values are physically consistent and show good agreement with standard observational results for compact objects. The characteristics of the redshift parameter support the realistic description of stable interior stellar structures of anisotropic strange quark objects in the alternative gravity theory.

Finally, we assess the physical viability of the spacetime model using another important structural property, namely the moment of inertia, which governs the dynamical behavior of the fluid distribution within the stellar interior and can be investigated using the mathematical formulation proposed in [174].

CPC Accepted

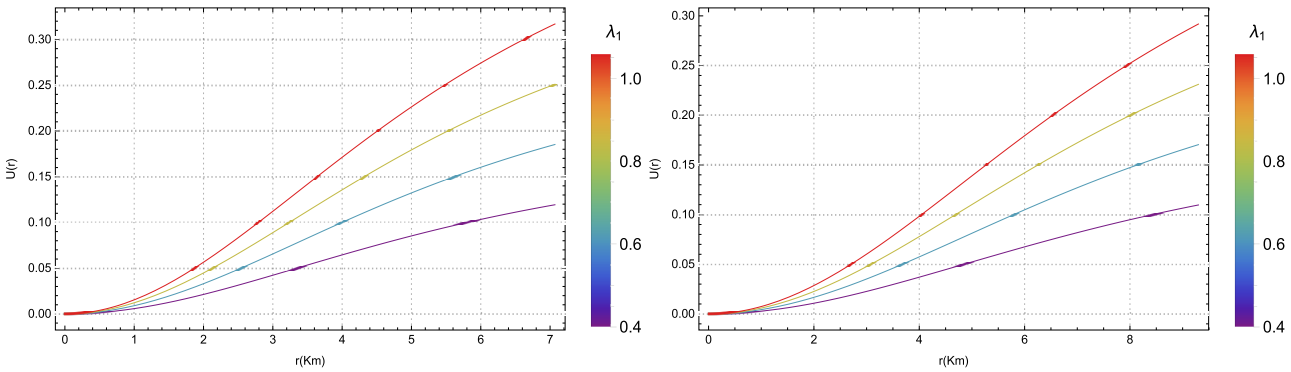

Fig. 20. (color online) Physical behavior of the compactification factor as a function of the radial coordinate r for two viable compact stellar models, $SAXJ1808.4-3658$ and $4U\ 1608-52$.

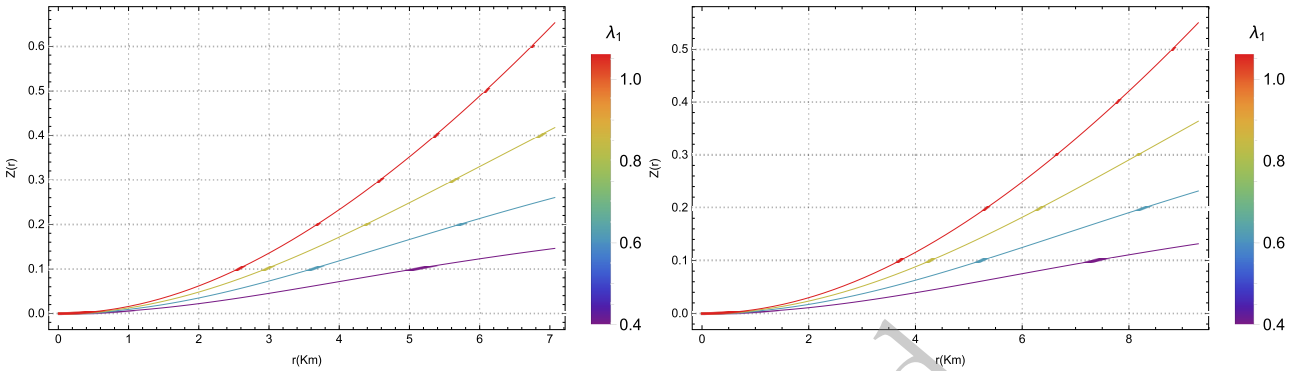

Fig. 21. (color online) Profiles of the redshift parameter as functions of the radial distance r for two well-known compact objects, $SAXJ1808.4-3658$ and $4U\ 1608-52$.

$$I=\frac{2}{5}\left[\left(1+\frac{M}{R}\right)MR^2\right]. \tag{68}$$

● We examine the structural and evolutionary behavior of the proposed strange quark star models by analyzing the moment of inertia, as illustrated in Fig. 22. The moment-of-inertia profiles exhibit rapid evolutionary variation while maintaining internal stability and non-singularity throughout the stellar configuration. The moment of inertia increases outward from the central core with increasing mass, reaching its maximum value when the mass M attains its optimum (see Fig. 22). This condition further confirms the model's stability and physical viability for describing the structural and evolutionary characteristics of compact objects composed of anisotropic strange quark matter.

VII. CONCLUSIONS

In the context of $f(\mathfrak{T})$ gravity, we have explored the construction of a stellar model based on the Finch–Skea metric potential. We examined the stellar structure to ensure the regularity of the metric potentials and the physical consistency of compact stellar objects. To investigate the physical properties of the compact model, we considered a specific linear teleparallel model of the form $f(\mathfrak{T})=\lambda_1\mathfrak{T}+\lambda_2$. For the quark matter distribution in the anisotropic compact model, we selected the MIT bag model equation of state (EoS), with B_g as the bag constant in units of MeV/fm^3. The Darmois junction conditions were also used to determine the values of the constants. To better capture the effects of the parameters λ_1 and λ_2 on the physical characteristics of the developed model, we used the vanishing radial pressure condition to determine the radii of the proposed stellar models. It is important to emphasize that the dependence of the stellar attributes on the parameter λ_1 should be interpreted in terms of its role in determining the effective gravitational coupling, rather than as evidence of an independent nonlinear torsion effect. Similarly, the parameter λ_2 contributes a constant geometric term to the field equations and affects the equilibrium configuration through its interplay with the matter distribution and boundary conditions. The resulting variations in density, pressure, mass, and compactness therefore demonstrate the response of the adopted stellar model to these effective gravitational parameters. The principal contribution of this analysis lies in the analytical construction of the stellar configuration and its systematic physical evaluation, rather than in establishing new gravitational degrees of freedom bey-

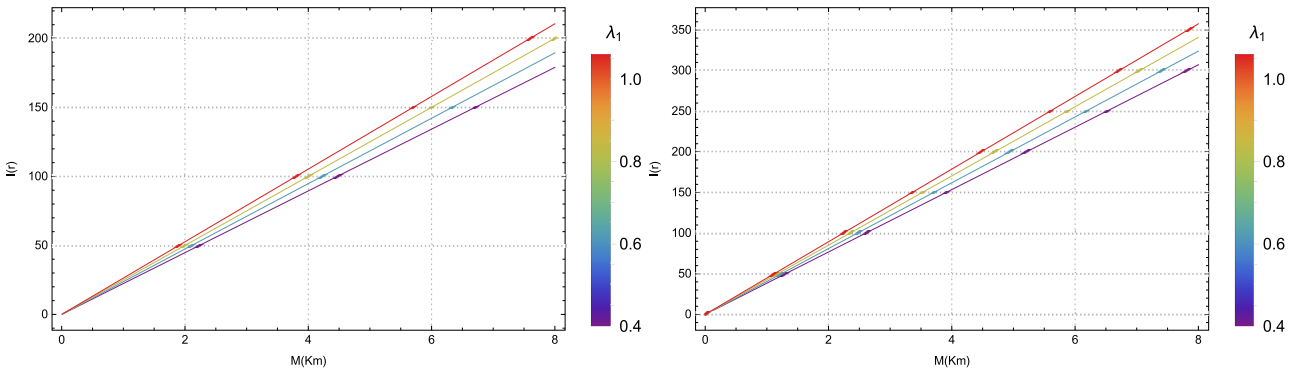

Fig. 22. (color online) Variation of the moment of inertia with M for two viable strange quark compact star candidates, $Cen\ X-3$ and $PSR\ J1903+327$.

CPC Accepted

ond *GR*. The primary findings are listed below.

● Figure 1 illustrates the consistent and regular behavior of the geometric components across the interior and exterior spacetimes for two well-known compact-star candidates, namely $SAXJ1808.4-3658$ and $4U1608-52$. The role of the bag constant in the possible formation of compact objects is examined in Fig. 2 by analyzing its evolution with respect to the theoretical parameter λ_1.

● Figures 3–5 show the graphical behavior of the pressure components and energy density for a physical compact model. For various values of λ_1, the radial and tangential pressures and the energy density remain positive, attain their maximum values at the stellar center, and gradually decrease toward the surface. As λ_1 increases, all fluid variables also increase, and the radial pressure vanishes at the boundary. Hence, our stellar model is physically sound.

● The regularity conditions for our model are examined and verified in Fig. 6. They vanish at the center and are negative elsewhere. Furthermore, the EoS parameters, shown in Figs. 7 and 8, remain within the interval [0, 1], indicating the existence of a physically acceptable stellar model.

● All energy conditions are satisfied throughout the radial coordinate domain, as illustrated in Fig. 9. Employing the Finch–Skea metric potential within the $f(\mathfrak{T})$ gravity formalism guarantees a regular matter distribution for both considered stars.

● The anisotropic force governs the pressure distribution: when $P_t > P_r$, the anisotropic pressure acts outward, whereas when $P_t < P_r$, it acts inward within the star. As shown in Fig. 10, the anisotropy factor is plotted as a function of the radial coordinate for different values of λ_1. The anisotropic stress vanishes at the stellar center for both configurations, as required by regularity. For $SAXJ1808.4-3658$, Δ remains non-negative throughout the interior and attains its maximum at $r \approx 5.8$. In contrast, for $4U1608-52$, the anisotropy factor is negative in the inner core and positive in the outer region; thus, the anisotropy changes sign inside the star. In both cases, the magnitude of anisotropy remains finite and small compared with the characteristic pressure scales, and the positive outer region provides the dominant anisotropic support against gravity.

● For a compact star to be stable, both the radial and transverse sound speeds must satisfy the causality conditions $0 \le v_r^2 = \frac{dP_r}{d\rho} \le 1$ and $0 \le v_t^2 = \frac{dP_t}{d\rho} \le 1$. The mathematical formulation of the Abreu-Herrera cracking condition is $v_t^2 - v_r^2 \le 0$, together with the bound $\left|v_t^2 - v_r^2\right| \le 1$. The behaviors of v_r^2, v_t^2, and their signed and absolute differences are illustrated in Figs. 11-13, respectively. These figures show that the squared radial sound speed remains constant at $\frac{1}{3}$ throughout the stellar interior. This behavior persists for all values of the parameter λ_1. However, v_t^2 decreases noticeably near the center and then increases again (see Fig. 11). As shown in Fig. 13, the quantity $\left|v_t^2 - v_r^2\right|$ remains positive throughout the radial coordinate and varies with increasing distance from the stellar center for the considered range of λ_1 values. In contrast, the signed difference $v_t^2 - v_r^2$ identifies regions that do not satisfy the condition associated with the absence of potentially cracking-prone regions (see Fig. 12). Thus, Figs. 11-13 demonstrate that the spacetime configurations satisfy the causality conditions and the bound on the absolute difference between the squared sound speeds, indicating physical admissibility. However, the signed difference $v_t^2 - v_r^2$ is not consistently compatible with the no-cracking condition because potentially cracking-prone regions emerge.

● The variations of all forces are plotted in Fig. 14, which shows that their net sum is zero at every radial position. Therefore, the proposed quark stellar model is in hydrostatic equilibrium.

● To investigate the stability of an anisotropic compact star, we analyze the adiabatic index (Γ), as defined in Eqs. (59) and (60). In the Newtonian limit, an isotropic fluid distribution remains stable if $\Gamma > \frac{4}{3}$ and becomes unstable otherwise. The present model satisfies this stability condition, as shown in Figs. 15 and 16, indicating a stable configuration.

● Figure 17 displays the mass profiles as functions of the central energy density, showing a direct relationship. This mass–central-density relation increases monotonically with central density throughout the entire configuration, reflecting the consistency and regularity of the resulting spacetime solution. Figure 18 shows the Zel'dovich static stability criterion, according to which the derivative of the mass with respect to the central density must be positive for a stable model. The consistent behavior and physical admissibility of the resulting profiles, which remain positive and finite, confirm that this condition is satisfied and further support our stability analysis.

● The plots of $M(r)$ are shown in Fig. 19. For different values of λ_1, the mass remains positive and regular at the stellar center and increases outward toward the surface. As λ_1 increases, the mass function also increases. Using the mass and radius, the compactness parameter is defined as their ratio, with an upper bound of $\frac{4}{9}$. Figure

CRC Accepted

20 shows the behavior of the compactness factor. For various values of the parameter, this factor remains positive and increases monotonically with the radial coordinate. This satisfies the required condition for a viable compact star model. Figure 21 displays the behavior of the surface redshift. We observe that this parameter is zero at the center and increases as we move outward from the core of the compact star model.

- Figure 22 shows a direct relationship between the moment of inertia and the total mass for all values of the parameter λ_1. Moreover, increasing this parameter results in a progressively larger moment of inertia.

In conclusion, our study employed the Finch–Skea spacetime to construct and analyze an anisotropic stellar configuration in teleparallel gravity. Exact solutions of the field equations were obtained, with the parameters determined from the boundary conditions, and their physical acceptability was evaluated through detailed graphical analysis. The results demonstrate the viability and well-behaved nature of the two pulsar candidates, which satisfy fundamental physical requirements, including positive energy density, finite pressures in the stellar interior, stability under different forces and adiabatic perturbations, and the causality conditions. They also show how realistic compact stellar configurations can be represented within the teleparallel gravity framework, providing insight into the roles of spherical geometry and anisotropy in this gravitational framework. This work motivates further investigations of other modified theories for astrophysical applications and contributes to a better understanding of compact stellar objects.

DECLARATION OF INTEREST

The authors declare that they have no known competing financial interests or personal relationships that could have appeared to influence the work reported in this paper.

ACKNOWLEDGEMENT

We sincerely thank the reviewers for their valuable and constructive suggestions, which helped improve the clarity and quality of the manuscript.

CPC Accepted

References

[1] S. Weinberg, Rev. Mod. Phys. **61**, 1 (1989)
[2] P. Brax, Rep. Prog. Phys. **81**, 016902 (2017)
[3] T. Clifton, P. G. Ferreira, A. Padilla, *et al*., Phys. Rep. **513**, 1 (2012)
[4] S. Nojiri, S. D. Odintsov, Phys. Rept. **505**, 59 (2011)
[5] S. Capozziello, M. De Laurentis, Phys. Rep. **509**, 167 (2011)
[6] S. Nojiri, S. D. Odintsov, V. K. Oikonomou, Phys. Rep. **692**, 1 (2017)
[7] T. P. Sotiriou, V. Faraoni, Rev. Mod. Phys. **82**, 451 (2010)
[8] S. D. Odintsov, V. K. Oikonomou, I. Giannakoudi, *et al*., Symmetry **15**, 1701 (2023)
[9] A. de la Cruz-Dombriz, D. Saez-Gomez, Entropy **14**, 1717 (2012)
[10] P. Feola, X. J. Forteza, S. Capozziello, *et al*., Phys. Rev. D **101**, 044037 (2020)
[11] S. Capozziello, M. De Laurentis, R. Farinelli, *et al*., Phys. Rev. D **93**, 023501 (2016)
[12] D. D. Doneva, S. S. Yazadjiev, N. Stergioulas, *et al*., Phys. Rev. D **98**, 104039 (2018)
[13] S. S. Yazadjiev, D. D. Doneva, K. D. Kokkotas, Eur. Phys. J. C **78**, 818 (2018)
[14] S. D. Odintsov, V. K. Oikonomou, Phys. Rev. D **107**, 104039 (2023)
[15] S. S. Yazadjiev, D. D. Doneva, K. D. Kokkotas, Phys. Rev. D **96**, 064002 (2017)
[16] D. D. Doneva, S. S. Yazadjiev, K. D. Kokkotas, Phys. Rev. D **92**, 064015 (2015)
[17] S. S. Yazadjiev, D. D. Doneva, K. D. Kokkotas, Phys. Rev. D **91**, 084018 (2015)
[18] K. V. Staykov, D. D. Doneva, S. S. Yazadjiev, *et al*., J. Cosmol. Astropart. Phys. **10**, 006 (2014)
[19] S. S. Yazadjiev, D. D. Doneva, K. D. Kokkotas, *et al*., J. Cosmol. Astropart. Phys. **06**, 003 (2014)
[20] T. Naseer, M. Sharif, Eur. Phys. J. C **84**, 554 (2024)
[21] T. Naseer, M. Sharif, Phys. Dark Univ. **46**, 101595 (2024)
[22] J. Santos, J. S. Alcaniz, F. C. Carvalho, *et al*., Phys. Lett. B **669**, 14 (2008)
[23] T. Harko, Phys. Lett. B **669**, 376 (2008)
[24] S. Capozziello, S. Nojiri, S. D. Odintsov, Phys. Lett. B **781**, 99 (2018)
[25] A. V. Astashenok, S. Capozziello, S. D. Odintsov, Astrophys. Space Sci. **355**, 333 (2015)
[26] A. V. Astashenok, S. Capozziello, S. D. Odintsov, J. Cosmol. Astropart. Phys. **12**, 040 (2013)
[27] R. Goswami, A. M. Nzioki, S. D. Maharaj, *et al*., Phys. Rev. D **90**, 084011 (2014)
[28] K. Hayashi, Phys. Lett. B **69**, 441 (1977)
[29] K. Hayashi, T. Shirafuji, Phys. Rev. D **19**, 3524 (1979)
[30] K. Hayashi, T. Shirafuji, Phys. Rev. D **24**, 3312 (1981)
[31] R. Ferraro, F. Fiorini, Phys. Rev. D **78**, 124019 (2008)
[32] F. Fiorini, R. Ferraro, Int. J. Mod. Phys. A **24**, 1686 (2009)
[33] S. Bahamonde, M. Wright, Phys. Rev. D **92**, 084034 (2015)
[34] S. Bahamonde, C. G. Böhmer, M. Wright, Phys. Rev. D **92**, 104042 (2015)
[35] G. Mustafa, S. K. Maurya, I, *et al*., Fortschr. Phys. **71**, 2200119 (2023)
[36] G. Mustafa, X. Gao, F. Javed, Fortschr. Phys. **70**, 2200053 (2022)
[37] G. G. L. Nashed, K. Bamba, Prog. Theor. Exp. Phys. **2022**, 103E01 (2022)
[38] G. G. L. Nashed, Class. Quantum Grav. **38**, 125004 (2021)
[39] G. Mustafa, M. Ahmad, Ö. Ali, *et al*. , Fortschr. Phys. **69**, 2100048 (2021)
[40] M. Pace, J. L. Said, Eur. Phys. J. C **77**, 62 (2017)

[41] A. Caliskan, R. M. Zulqarnain, E. GÜdekli, *et al.* , Front. Astron. Space Sci. **10**, 1203777 (2023)
[42] R-H. Lina, X-N. Chen, X-H. Zhai, Eur. Phys. J. C **82**, 308 (2022)
[43] R. Saleem, F. Kramat M. Zubair, Phys. Dark Univ. **30**, 100592 (2020)
[44] H. Nazar, G. Abbas, A. Abbas, *et al.*, Fortschr. Phys. **72**, 2300250 (2024)
[45] H. Nazar, G. Abbas, Chin. J. Phys. **79**, 124 (2022)
[46] E. GÜdekli, H. Nazar, G. Abbas, *et al.* , Int. J. Geom. Meth. Mod. Phys. **19**, 2250227 (2022)
[47] R. Ahmed, G. Abbas, H. Nazar, *et al.*, Int. J. Geom. Meth. Mod. Phys. **19**, 2250170 (2022)
[48] G. Abbas, H. Nazar, Ann. Phys. **424**, 168336 (2021)
[49] G. Abbas, H. Nazar, Eur. Phys. J. C **78**, 957 (2018)
[50] H. Nazar, G. Abbas, Advan. Astron. **2021**, 6698208 (2021)
[51] H. Nazar, Ali H. Alkhaldi, G. Abbas, *et al.*, Int. J. Mod. Phys. A **36**, 2150233 (2021)
[52] A. Majeed, H. Nazar, G. Abbas, Chin. J. Phys. **86**, 530 (2023)
[53] S. K. Maurya, A. Errehymy, D. Deb, *et al.*, Phys. Rev. D **100**, 044014 (2019)
[54] G. Mustafa, S. K. Maurya, S. Ray, Astrophys. J. **941**, 170 (2022)
[55] M. Rahaman, Ksh. N. Singh, A. Errehymy, *et al.*, Eur. Phys. J. C **80**, 272 (2020)
[56] G. Mustafa, M. F. Shamir, X. Tie-Cheng, Phys. Rev. D **101**, 104013 (2020)
[57] S. K. Maurya, G. Mustafa, M. Govender, *et al.*, J. Cosmol. Astropart. Phys. **10**, 003 (2022)
[58] C. G. Boehmer, T. Harko, F. S. N. Lobo, Phys. Rev. D **85**, 044033 (2012)
[59] R. Ferraro, F. Fiorini, Phys. Rev. D **84**, 083518 (2011)
[60] A. V. Astashenok, S. D. Odintsov, Mon. Not. Roy. Astron. Soc. **498**, 3616 (2020)
[61] J. M. Z. Pretel, S. E. Joŕas, R. R. R. Reis, *et al.* , J. Cosmol. Astropart. Phys. **08**, 055 (2021)
[62] B. Siza, *et al.*, Eur. Phys. J. C **84**, 1203 (2024)
[63] T. Naseer, Astropart. Phys. **166**, 103073 (2025)
[64] J. Andrade, *et al.*, Eur. Phys. J. C **85**, 598 (2025)
[65] T. Naseer, Int. J. Geom. Methods Mod. Phys. **22**, 2550143 (2025)
[66] M. Sharif, T. Naseer, A. Raza, Eur. Phys. J. C **86**, 980 (2026)
[67] T. Naseer, M. Sharif, A. Raza, Ann. Phys. **494**, 170658 (2026)
[68] S. Bahamonde, K. F. Dialektopoulos, C. Escamilla-Rivera, *et al.*, Rep. Prog. Phys. **86**, 026901 (2023)
[69] J. Solanki, J. L. Said, Eur. Phys. J. C **82**, 35 (2022)
[70] A. Ditta, M. Ahmad, I. Hussain, *et al.*, Chin. Phys. C **45**, 045102 (2021)
[71] M. H. Daouda, M. E. Rodrigues, M. J. S. Houndjo, Phys. Lett. B **715**, 241 (2012)
[72] M. Zubair, G. Abbas, Astrophys. Space Sci. **361**, 27 (2016)
[73] G. G. L. Nashed, E. N. Saridakis, J. Cosmol. Astropart. Phys. **05**, 017 (2022)
[74] D. Deb, S. Ghosh, S.K. Maurya, *et al.*, Tech Vistas. **1**, 1 (2018)
[75] S. Ilijić, M. Sossich , Phys. Rev. D **98**, 064047 (2018)
[76] G. Abbas, A. Kanwal, M. Zubair, Astrophys. Space Sci. **357**, 109 (2015)
[77] D. Momeni, G. Abbas, S. Qaisar, *et al.*, Can. J. Phys. **96**, 1295 (2018)
[78] G. Abbas, S. Qaisar, A. Jawad, *et al.*, Astrophys. Space Sci. **359**, 57 (2015)
[79] S. Ilijić, M. Sossich , Phys. Rev. D **102**, 084019 (2020)
[80] J. C. N. de Araujo, H. G. M. Fortes, Braz. J. Phys. **53**, 75 (2023)
[81] J. C. N. de Araujo, H. G. M. Fortes, Int. J. Mod. Phys. D **31**, 2250101 (2022)
[82] J. C. N. de Araujo, H. G. M. Fortes, Eur. Phys. J. C **83**, 376 (2023)
[83] J. C. N. de Araujo, H. G. M. Fortes, Eur. Phys. J. C **83**, 1168 (2023)
[84] S. G. Vilhena, S. B. Duarte, M. Dutra, *et al.*, J. Cosmol. Astropart. Phys. **04**, 044 (2023)
[85] M. G. Ganiou, C. Aïnamon, M. J. S. Houndjo, *et al.* , Eur. Phys. J. Plus **132**, 250 (2017)
[86] G. G. L. Nashed, S. Capozziello, Eur. Phys. J. C **80**, 969 (2020)
[87] P. Bhar, Chin. J. Phys. **83**, 61 (2023)
[88] M. Sharif, A. Waseem, Astrophys. Space Sci. **361**, 27 (2016)
[89] M. Zubair, A. Ditta, G. Abbas, *et al.*, Chin. Phys. C **45**, 085102 (2021)
[90] R. Saleem, M. Zubair, M. I. Aslam, *et al.*, Int. J. Geom. Meth. Mod. Phys. **21**, 2450044 (2024)
[91] H. Sohail, A. Ditta, I. Mahmood, *et al.*, Eur. Phys. J. Plus **139**, 695 (2024)
[92] S. Pradhan, P. Bhar, S. Mandal, *et al.*, arXiv: 2408.03967v1.
[93] S. Rani, M. B. Amin, A. Jawad, Eur. Phys. J. Plus **131**, 436 (2016)
[94] T. Naseer, H. Afzal, M. Sharif, *et al.*, Nucl. Phys. B **1027**, 117465 (2026)
[95] S. Sadiq, A. Atif, F. Javed, *et al.*, Chin. J. Phys. **90**, 594 (2024)
[96] T. Naseer, M. Sharif, M. Waqas, *et al.*, Mod. Phys. Lett. A **41**, 2650058 (2026)
[97] C. Li, Y. Cai, Y. Cai, *et al.*, J. Cosmol. Astropart. Phys **10**, 001 (2018)
[98] Y.-F. Cai, C. Li, E. N. Saridakis, *et al.*, Phys. Rev. D **97**, 103513 (2018)
[99] S.-F. Yan, P. Zhang, J.-W. Chen, *et al.*, Phys. Rev. D **101**, 121301 (2020)
[100] G. Farrugia, J. L. Said, V. Gakis, *et al.*, Phys. Rev. D **97**, 124064 (2018)
[101] S. Bahamonde, K. Flathmann, C. Pfeifer, Phys. Rev. D **100**, 084064 (2019)
[102] K. Bamba, S. Nojiri, S. D. Odintsov, Phys. Lett. B **731**, 257 (2014)
[103] R. C. Nunes, M. E. S. Alves, J. C. N. de Araujo, Phys. Rev. D **100**, 064012 (2019)
[104] R. C. Nunes, S. Pan, E. N. Saridakis, Phys. Rev. D **98**, 104055 (2018)
[105] J. Jeans, Mon. Not. R. Astron. Soc. **82**, 122 (1922)
[106] M. Ruderman, Annu. Rev. Astron. Astrophys. **10**, 427 (1972)
[107] V. Canuto, Annu. Rev. Astron. Astrophys. **12**, 167 (1974)
[108] S. S. Yazadjiev, Phys. Rev. D **85**, 044030 (2012)
[109] C. Y. Cardall, M. Prakash, J. M. Lattimer, Astrophys. J. **554**, 322 (2001)
[110] V. Ioka, M. Sasaki, Astrophys. J. **600**, 296 (2004)
[111] R. Ciolfi, V. Ferrari, L. Gualtieri, Mon. Not. R. Astron. Soc. **406**, 2540 (2010)

CPC Accepted

[112] R. F. Sawyer, Phys. Rev. Lett. **29**, 382 (1972)
[113] H. Heiselberg, M. Hjorth-Jensen, Phys. Rep. **328**, 237 (2000)
[114] R. L. Bowers, E. P. T. Liang, Astrophys. J. **188**, 657 (1974)
[115] M. Sharif, T. Naseer, Eur. Phys. J. Plus **139**, 296 (2024)
[116] R. Sharma, S. D. Maharaj, Mon. Not. R. Astron. Soc. **375**, 1265 (2007)
[117] M. Govender, S. Thirukkanesh, Astrophys. Space Sci. **358**, 39 (2015)
[118] F. Tello-Ortiz, M. Malaver, Á. Rincón, *et al*., Eur. Phys. J. C **80**, 371 (2020)
[119] S. Hansraj, L. Moodly, Eur. Phys. J. C **80**, 496 (2020)
[120] E. Contreras, Z. Stuchlik, Eur. Phys. J. C **82**, 706 (2022)
[121] G. R. Bengochea, R. Ferraro, Phys. Rev. D **79**, 124019 (2009)
[122] B. Li, T. P. Sotiriou, J. D. Barrow, Phys. Rev. D **83**, 064035 (2011)
[123] C. Deliduman and B. Yapiskan.: arXiv: 1103.2225
[124] M. R. Finch, J. E. F. Skea, Class. Quantum Grav. **6**, 467 (1989)
[125] H. L. Duorah, R. Ray, Class. Quantum Grav. **4**, 1691 (1987)
[126] M. S. R. Delgaty, K. Lake, Comp. Phys. Communic. **115**, 395 (1998)
[127] S. Hansraj, S. D. Maharaj, Int. J. Mod. Phys. D **15**, 1311 (2006)
[128] R. Sharma, B. S. Ratanpal, Int. J. Mod. Phys. D **22**, 1350074 (2013)
[129] D. M. Pandya, V. O. Thomas, R. Sharma, Astrophys. Space Sci. **356**, 285 (2015)
[130] R. Sharma, S. Das, J. Gravity **2013**, 659605 (2013)
[131] M. Kalam, F. Rahaman, M. Molla, *et al*., Astrophys. Space Sci. **349**, 865 (2014)
[132] Z. Yousaf, U. A. Khokhar, J. Rayimbaev, *et al*., Nucl. Phys. B **1023**, 117317 (2026)
[133] P. Rej, R. S. Bogad, M. Govender, Chin. J. Phys. **87**, 608 (2024)
[134] H. Nazar, M. Azam, G. Abbas, *et al*., Chin. Phys. C **47**, 035109 (2023)
[135] A. Jangid, B. S. Ratanpal, K. K. Venkataratnam, Gravit. Cosmol. **29**, 206 (2023)
[136] O. Sokoliuk, A. Baransky, P. K. Sahoo, Chin. Phys. C **47**, 015104 (2023)
[137] M. Malaver, R. Iyer, Can. J. Pure. Appl. Sci. **16**, 5531 (2022)
[138] M. F. Shamir, G. Mustafa, M. Ahmad, Nuc. Phys. B **967**, 115418 (2021)
[139] R. Naeem, M. Azam, G. Abbas, *et al*., New Astron. **89**, 101651 (2021)
[140] S. Dey, B. C. Paul, Class. Quantum Grav. **37**, 075017 (2020)
[141] A. Chanda, S. Dey, B. C. Paul, Eur. Phys. J C **79**, 502 (2019)
[142] S. Hansraj, Eur. Phys. J. C **77**, 557 (2017)
[143] N. Dadich, S. Hansraj, B. Chilambwe, Int. J. Mod. Phys. D **26**, 1750056 (2017)
[144] A. Molina, N. Dadich, A. Khugaev, Gen. Relativ. GRavit. **49**, 96 (2017)
[145] S. K. Maurya, F.Tello-Ortiz, Eur. Phys. J. C **79**, 33 (2019)
[146] K. N. Singh, S. K. Maurya, A. Dutta, *et al*., Eur. Phys. J. C **81**, 909 (2021)
[147] S. K. Maurya, F. Tello-Ortiz, S. Ray, Phys. Dark Univ. **31**, 100753 (2021)
[148] K. N. Singh, S. K. Maurya, A. Errehymy, *et al*., Phys. Dark Univ. **30**, 100620 (2020)
[149] S. D. Maharaj, D. K. Matondo, P. M. Takisa, Int. J. Mod. Phys. D **26**, 1750014 (2016)
[150] R. Sharma, S. Das, S. Thirukkanesh, Astrophys. Space Sci. **362**, 232 (2017)
[151] C. Alcock, E. Farhi, A. Olinto, Astrophys. J. **310**, 216 (1986)
[152] E. Farhi, R. L. Jaffe, Phys. Rev. D **30**, 2379 (1984)
[153] A. Chodos, R. L. Jaffe, K. Johnson, *et al*., Phys. Rev. D **9**, 3471 (1974)
[154] T. Naseer, M. Sharif, Phys. Scr. **99**, 095028 (2024)
[155] M. Jasim, D. Deb, S. Ray, *et al*., Eur. Phys. J. C **78**, 603 (2018)
[156] N. Stergioulas, Living Rev. Relativ. **6**, 3 (2003)
[157] K. Schwarzschild, Sitzbcr (Press. Akad. Wiss., Berlin, 1916), p.189.
[158] N. K. Glendenning, Compact Stars: Nuc. Phys. Particle Physics and General Relativity, second edn. (Springer, New York, 2000).
[159] M. Herzog, F. K. Röpke , Phys. Rev. D **84**, 083002 (2011)
[160] D. Shee, F. Rahaman, B. K. Gupta, *et al*., Astrophys. Space Sci. **361**, 167 (2016)
[161] A. V. Astashenok, AIP Conf. Proc. **1606**, 99 (2014)
[162] Sk. M. Hossein, F. Rahaman, J. Naskar, *et al*., Int. J. Mod. Phys. D **21**, 1250088 (2012)
[163] L. Herrera, G. J. Ruggeri, L. Witten, Astrophys. J. **234**, 1094 (1979)
[164] L. Herrera, Phys. Lett. A **165**, 206 (1992)
[165] S. Capozziello, O. Luongo, L. Mauro, Eur. Phys. J. Plus **136**, 167 (2021)
[166] R. Chan, L. Herrera, N. O. Santos, Mon. Not. R. Astron. Soc. **265**, 533 (1993)
[167] H. Abreu, H. Hernández, L. A. Núñez, Class. Quant. GRavit. **24**, 4631 (2007)
[168] H. Andréasson, Comm. Math. Phys. **288**, 715 (2009)
[169] S. Chandrasekhar, Phys. Rev. Lett. **12**(4), 114 (1964)
[170] B.K. Harrison, K.S. Thorne, M. Wakano, *et al*., Gravitation Theory and Gravitational Collapse, University of Chicago Press, 1965.
[171] Y.B. Zeldovich, I.D. Novikov, 1, University of Chicago Press, 1971.
[172] K. Jotania, R. Tikekar, Int. J. Mod. Phys. D **15**, 1175 (2006)
[173] H. A. Buchdahl, Phys. Rev. **116**, 1027 (1959)
[174] D. G. Ravenhall, C. J. Pethick, Astrophys. J. **424**, 846 (1994)

CPC Accepted